Multibreathers in Klein-Gordon chains with interactions beyond nearest neighbors

V. Koukouloyannis[a,*], P.G. Kevrekidis[b], J. Cuevas[c], V. Rothos[d]

[a] *Department of Civil Engineering, Technological Educational Institute of Serres, 62124 Serres, Greece*
[b] *Department of Mathematics and Statistics, University of Massachusetts, Amherst MA 01003-4515*
[c] *Nonlinear Physics Group. Departamento de Física Aplicada I, Escuela Politécnica Superior. Universidad de Sevilla. C/ Virgen de África, 7, 41011 Sevilla, Spain*
[d] *Department of Mathematics, Faculty of Engineering, Aristotle University of Thessaloniki,Thessaloniki GR54124 Greece*

Abstract

We study the existence and stability of multibreathers in Klein-Gordon chains with interactions that are not restricted to nearest neighbors. We provide a general framework where such long range effects can be taken into consideration for arbitrarily varying (as a function of the node distance) linear couplings between arbitrary sets of neighbors in the chain. By examining special case examples such as three-site breathers with next-nearest-neighbors, we find *crucial* modifications to the nearest-neighbor picture of one-dimensional oscillators being excited either in- or anti-phase. Configurations with nontrivial phase profiles emerge from or collide with the ones with standard (0 or π) phase difference profiles, through supercritical or subcritical bifurcations respectively. Similar bifurcations emerge when examining four-site breathers with either next-nearest-neighbor or even interactions with the three-nearest one-dimensional neighbors. The latter setting can be thought of as a prototype for the two-dimensional building block, namely a square of lattice nodes, which is also examined.

1. Introduction

The initial numerical inception of anharmonic modes consisting of a few excited sites in nonlinear lattices [1, 2], and their subsequent placement on a rigorous existence basis (under rather generically satisfied non-resonance conditions) in [3] has triggered a huge growth of interest in the theme of the so-called discrete breathers. These are exponentially localized in space, periodic in time states which have subsequently been theoretically/numerically predicted and experimentally verified to arise in a very diverse host of applications. These include (but are not limited to) DNA double-strand dynamics in biophysics [4], coupled waveguide arrays and photorefractive crystals in nonlinear optics [5, 6, 7], breathing oscillations in micromechanical cantilever arrays [8], Bose-Einstein condensates in optical lattices in atomic physics [9], and granular crystals [10]. The interest in this theme has also been mirrored in a wide array of reviews on methods of identifying and analyzing such intrinsically localized modes [11, 12, 13, 14].

More recently, the stability of the discrete breather configurations, especially in the case of the excitation of multiple sites has been of particular interest. One approach to obtaining relevant results consists of the so-called Aubry band theory [14], used e.g. in [15, 16]. This led to the conclusion that for soft nonlinear potentials multi-breathers with any subset of adjacent sites being excited in-phase are unstable, while ones with all adjacent sites in anti-phase can be stable in the vicinity of the so-called anti-continuum limit of uncoupled anharmonic oscillators. A complementary theory that yields insights on both the existence and the stability of multibreathers has been pioneered by MacKay and collaborators; see e.g., [17, 18, 19]. This is the so-called effective Hamiltonian method which is identified by averaging over the period of the

*Corresponding author
Email address: vkouk@physics.auth.gr (V. Koukouloyannis)

unperturbed solution and developing the proper action-angle variables. The extrema of the resulting effective Hamiltonian determine the relative phases of adjacent excited sites in the multi-site breather solution, while the relevant Hessian is intimately connected to the Floquet multipliers of the associated periodic orbit. Using this methodology, the work of [20] retrieved as well as refined the results of [15] for arbitrary phase relations between the excited oscillators of such multi-breather configurations. The equivalence between these two basic methods and their conclusions was recently established in [21]. We should also note in passing that similar results have been acquired also in configurations where there are "holes" between the excited breather sites [22], through higher order perturbation theory generalizing the above conclusions to the cases with one-site holes. On the other hand, the existence and stability of single/multi-site breathers have been studied in diatomic FPU lattices. The work of [23] was based on a discrete Sturm theorem which necessitated (for the separation of the space n and time t variables) a potential which was at least purely quartic. In the realm of lattices with longer than the nearest-neighbor interactions a variety of issues have been considered such as, e.g. in [24], the existence and bifurcation of quasi periodic traveling waves in nonlocal lattices with polynomial type potentials.

In the present work, we consider the generalization of the above settings, which are principally concerned with the interaction between nearest neighbors, to the case with longer range neighbor interactions for Klein-Gordon chains. Upon revisiting the nearest neighbor case and presenting the effective Hamiltonian formalism (of MacKay and collaborators) there (section II) for existence and stability of multibreathers, in section III, we generalize this formalism to the case of an arbitrary number of neighbors (denoted by r) interacting with each other. By specializing to the case of nearest and next-nearest neighbor interactions (and three-site breathers) as our first case example of the application of the results in section IV, we already infer the fundamental modifications to the standard picture that ensue due to interactions beyond nearest neighbors. These include configurations that have *non-standard relative phases between adjacent oscillators*, a feature which is absent in the nearest-neighbor interaction case [25] and also *symmetry breaking bifurcations* that arise due to the "collision" of branches of solutions with such non-trivial phase relations, with more standard ones with relative phases of 0 or π between adjacent oscillators. The generic nature of these conclusions is confirmed by considering the case examples of four-site breathers with next-nearest-neighbor interactions in section V and such breathers with interaction ranges of $r = 3$ in section VI. The latter setting is very close to genuinely two-dimensional setting in a square lattice plaquette, which constitutes our final example in section VII. We close our presentation by some remarks on the parallels of our results with the simpler case of the discrete nonlinear Schrödinger lattices [26] (section VIII), which has been examined earlier in [27, 28], as well as a summary of our conclusions and some future directions (section IX).

2. Background: The Classical Klein-Gordon chain

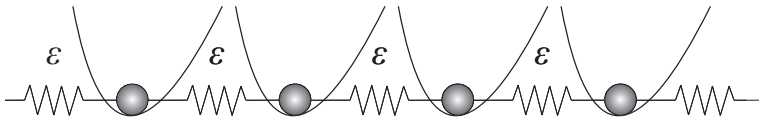

Figure 1: The classical nearest-neighbor Klein-Gordon chain

The Hamiltonian of a Klein-Gordon chain with nearest-neighbor (NN) interactions is the following

$$H = H_0 + \varepsilon H_1 = \sum_{i=-\infty}^{\infty} \left[\frac{1}{2} p_i^2 + V(x_i) \right] + \frac{\varepsilon}{2} \sum_{i=-\infty}^{\infty} \left(x_i - x_{i-1} \right)^2 , \tag{1}$$

which leads to the equations of motion

$$\ddot{x_i} = -V'(x_i) + \varepsilon(x_{i-1} - 2x_i + x_{i+1}).$$

It is well known that this system supports discrete breather, as well as, multibreather solutions. As indicated above, there are several papers dealing with the existence and stability of these motions; see e.g. [3, 29, 30, 31, 17, 15, 20, 22].

2.1. Persistence of mutibreathers

The derivation of the persistence conditions will be based on the notion of the *anticontinuum limit* and the results of [17]. In the anti-continuum limit $\varepsilon = 0$, we consider all the oscillators of the chain at rest except for $n+1$ "central" ones which move in periodic orbits of frequency ω, but arbitrary phases. This trivially space localized and time-periodic motion is denoted by $z_0(t)$ and let $\mathbb{S} = \{0, 1, \ldots, n\}$ the set of indices corresponding to the central oscillators. To these oscillators, we perform the action-angle $(x, p) \mapsto (w, J)$ canonical transformation. The Hamiltonian then becomes $H = H(w_i, J_i, x_j, y_j)$ with $i \in \mathbb{S}$ and $j \in \mathbb{Z} \setminus \mathbb{S}$. After that, we perform a second canonical transformation

$$\begin{aligned} \vartheta &= w_0 & A &= \sum_{j=0}^{n} J_j \\ \phi_i &= w_{i+1} - w_i & I_i &= \sum_{j=i}^{n} J_j \quad i = 1 \ldots n \end{aligned}$$

where ϕ_i denote the n phase differences between the $n+1$ successive oscillators and I_i are the conjugate generalized momenta. Using these variables, the Hamiltonian becomes $H = H(\phi_j, I_j, \vartheta, A, x_j, p_j)$. We define then

$$H^{\text{eff}}(\phi_i, I_i, A) = \oint H \circ z(t) \mathrm{d}t,$$

where $z(t)$ is periodic orbit obtained by a continuation procedure using constant symplectic "area" A. Since in H^{eff} the variable ϑ is ignorable by construction, the conjugate variable A will be a constant of motion. We expand all the variables involving in power series of ε and keep the leading order terms. In this level of approximation, $z(t)$ can be taken equal to $z_0(t)$. So, H^{eff} can be written as

$$H^{\text{eff}} = H_0(I_i) + \varepsilon \langle H_1 \rangle (\phi_i, I_i) \tag{2}$$

where we have omitted constant and higher order terms. The average value of the coupling part of the Hamiltonian is

$$\langle H_1 \rangle (\phi_i, I_i) = \frac{1}{T} \oint H_1(\vartheta, \phi_i, I_i) \mathrm{d}t$$

where all the calculations have been made along the unperturbed periodic orbit z_0.

In [17] it was proven that the critical points of the dynamical system associated with H^{eff} are in one-to-one correspondence with the periodic orbits of the original H-system which will be continued for ε nonzero but small enough to provide multibreathers. So, by using the form of H^{eff} of (2), we obtain the persistence conditions for the existence of $n+1$-site multibreathers as

$$\frac{\partial \langle H_1 \rangle}{\partial \phi_i} = 0, \quad i = 1 \ldots n, \tag{3}$$

Note that the persistence conditions are the same for every lattice case where the Hamiltonian can be written in the for $H = H_0 + \varepsilon H_1$ with $\frac{\partial \langle H_1 \rangle}{\partial \phi_i} \not\equiv 0$.

In order to obtain specific conditions about the configurations which persist for $\varepsilon \neq 0$, to provide multibreathers, we need to calculate $\langle H_1 \rangle$. The motion of the central oscillators for $\varepsilon = 0$ can be described by

$$x_i(w_i) = \sum_{m=0}^{\infty} A_m(J_i) \cos(m w_i). \tag{4}$$

Since the action J_i remains constant along an orbit in the anticontinuum limit, x_i depends only on w_i. So, the average value of H_1 becomes ([20] appendix A)

$$\langle H_1 \rangle = -\frac{1}{2} \sum_{m=1}^{\infty} \sum_{s=1}^{n} A_m^2 \cos(m \phi_s)$$

and the persistence conditions (3) become in the case of Klein-Gordon chains with nearest neighbor interactions,

$$\frac{\partial \langle H_1 \rangle}{\partial \phi_i} = 0 \Rightarrow M(\phi) \equiv \sum_{m=1}^{\infty} m A_m^2 \sin(m\phi_i) = 0, \quad i = 1 \dots n. \tag{5}$$

The function $M(\phi)$ possesses the obvious roots $\phi_i = 0, \pi$, while it has no others, as it is shown in [25][1]. Additionally, the resulting breather states are exponentially localized in space as it can be shown in the framework of [33].

2.2. Stability of multibreathers

The spectral stability of the above mentioned multibreather solutions or, equivalently, the linear stability of the corresponding periodic orbits is determined through its *characteristics exponents* σ_i. These exponents are connected with the corresponding Floquet multipliers by the relation

$$\lambda_i = e^{\sigma_i T},$$

where $T = 2\pi/\omega$ is the period of the multibreather. Due to the Hamiltonian character of the system there is a pair of exponents identically equal to zero. The non-zero characteristic exponents of the central oscillators correspond to the eigenvalues of the $(2n \times 2n)$ *stability matrix* [17] $\mathbf{E} = \mathbf{\Omega} D^2 H^{\text{eff}}$, where Ω is the matrix of the symplectic form $\mathbf{\Omega} = \begin{pmatrix} \mathbf{O} & -\mathbf{I} \\ \mathbf{I} & \mathbf{O} \end{pmatrix}$ and $\mathbf{I}$ is the $n \times n$ identity matrix. The effective Hamiltonian H^{eff}, as it has already been mentioned, in first order of approximation is given by $H^{\text{eff}} = H_0 + \varepsilon \langle H_1 \rangle$. So, the stability matrix $\mathbf{E}$, to leading order of approximation and by taking into consideration the form of H^{eff}, becomes

$$\mathbf{E} = \left(\begin{array}{c|c} \mathbf{A} & \mathbf{B} \\ \hline \mathbf{C} & \mathbf{D} \end{array} \right) = \left(\begin{array}{c|c} \varepsilon \mathbf{A_1} & \varepsilon \mathbf{B_1} \\ \hline \mathbf{C_0} + \varepsilon \mathbf{C_1} & \varepsilon \mathbf{D_1} \end{array} \right) = \left(\begin{array}{c|c} -\varepsilon \dfrac{\partial^2 \langle H_1 \rangle}{\partial \phi_i \partial I_j} & -\varepsilon \dfrac{\partial^2 \langle H_1 \rangle}{\partial \phi_i \partial \phi_j} \\ \hline \dfrac{\partial^2 H_0}{\partial I_i I_j} + \varepsilon \dfrac{\partial^2 \langle H_1 \rangle}{\partial I_i \partial I_j} & \varepsilon \dfrac{\partial^2 \langle H_1 \rangle}{\partial \phi_j \partial I_i} \end{array} \right). \tag{6}$$

Since the only possible solutions are the ones with $\phi_i = 0, \pi$ and we consider central sites oscillating with the same frequency ω, we get that $\mathbf{A_1} = \mathbf{D_1} = \mathbf{0}$ and so, the nonzero characteristic exponents are given to leading order of approximation by

$$\sigma_{\pm i} = \pm \sqrt{\varepsilon \, \chi_{1i}} + \mathcal{O}(\varepsilon^{3/2}) \quad i = 1 \dots n, \tag{7}$$

where χ_{1i} are the eigenvalues of the matrix $\mathbf{B_1} \cdot \mathbf{C_0}$. Due to the form of the $J \mapsto I$ transformation the $\mathbf{C_0}$ matrix becomes (see [20] appendix B)

$$\mathbf{C_0} = \frac{\partial^2 H_0}{\partial I_i \partial I_j} = -\frac{\partial \omega}{\partial J} \cdot \mathbf{L} = -\frac{\partial \omega}{\partial J} \cdot \begin{pmatrix} 2 & -1 & 0 & & \\ -1 & 2 & -1 & 0 & \\ & \ddots & \ddots & \ddots & \\ & 0 & -1 & 2 & -1 \\ & & 0 & -1 & 2 \end{pmatrix}.$$

So, (7) becomes, up to leading order terms,

$$\sigma_{\pm i} = \pm \sqrt{-\varepsilon \frac{\partial \omega}{\partial J} \chi_{z i}} \quad i = 1 \dots n, \tag{8}$$

[1] One could present the case of *phonobreathers* (see e.g. [32]) as a counterexample of this statement. But, these motions are substantially different from the multibreathers we study in this work, in the sense that, in the anticontinuoum limit, in the case of phonobreathers all the sites of the lattice are excited, while, in our case there is a specific number of $n+1$ central oscillators.

where $\chi_{z\,i}$ are the eigenvalues of $\mathbf{Z} = \mathbf{B_1} \cdot \mathbf{L}$.

For systems of the form (1) we get

$$\mathbf{B_1} = \frac{\partial^2 \langle H_1 \rangle}{\partial \phi_i \partial \phi_j} = \begin{cases} f_i & \text{for } i = j \\ 0 & \text{for } i \neq j \end{cases},$$

with

$$f_i = f(\phi_i) = \frac{1}{2} \sum_{m=1}^{\infty} m^2 A_m^2 \cos(m\phi_i). \tag{9}$$

So, $\mathbf{Z}$ can be written as

$$\mathbf{Z} = \mathbf{B_1} \cdot \mathbf{L} = \frac{\partial^2 \langle H_1 \rangle}{\partial \phi_i \partial \phi_j} \cdot \begin{pmatrix} 2 & -1 & 0 & & \\ -1 & 2 & -1 & 0 & \\ & \ddots & \ddots & \ddots & \\ & 0 & -1 & 2 & -1 \\ & & 0 & -1 & 2 \end{pmatrix} = \begin{pmatrix} 2f_1 & -f_1 & 0 & & \\ -f_2 & 2f_2 & -f_2 & 0 & \\ & \ddots & \ddots & \ddots & \\ & 0 & -f_{n-1} & 2f_{n-1} & -f_{n-1} \\ & & 0 & -f_n & 2f_n \end{pmatrix} \tag{10}$$

Note that, for linear stability we require all the Floquet multipliers to lie on the unit circle, which is tantamount to all the characteristic exponents being purely imaginary. This depends on the sign of $P = \varepsilon \frac{\partial \omega}{\partial J}$ and the sign of χ_z as it can be seen from (8). Finally, by using some counting theorems [20] for (10), we obtain:

Theorem 1. *[20] In systems of the form (1), if $P \equiv \varepsilon \frac{\partial \omega}{\partial J} < 0$ the only configuration which leads to linearly stable multibreathers, for $|\varepsilon|$ small enough, is the one with $\phi_i = \pi \quad \forall i = 1 \ldots n$ (anti-phase multibreather), while if $P > 0$ the only linearly stable configuration, for $|\varepsilon|$ small enough, is the one with $\phi_i = 0 \quad \forall i = 1 \ldots n$ (in-phase multibreather). Moreover, for $P < 0$ (respectively, $P > 0$), for unstable configurations, their number of unstable eigenvalues will be precisely equal to the number of nearest neighbors which are in- (respectively, in anti-) phase between them.*

Remark 1: Note that, the form of the matrix $\mathbf{C_0}$ is such due to the form of the $J \mapsto I$ transformation and the fact that in the anti-continuum limit $\frac{\partial H_0}{\partial J} = \omega$ and $\omega_i = \omega$ for $i = 1 \ldots n$. So, it is independent of the range of the interaction between the oscillators of the chain and it will remain the same in what follows. On the other hand, the diagonal form of $\mathbf{B_1}$ will change if longer range interactions are added to the system. So, the theorem will *no longer hold* but the general methodology will still apply and the characteristic exponents of the multibreather will be given by (8). We will consider this case in what follows.

Remark 2: In our previous works we used the term "out-of-phase" for $\phi = \pi$ configurations. This was because the only out-of-phase configuration was the $\phi = \pi$ one. In the present work, since, as we will see in the next section, there are out-of phase configurations with $\phi \neq \pi$, we use the term "anti-phase" for the $\phi = \pi$ configuration.

Remark 3: As indicated in [22], it is possible to generalize the stability considerations to the case where not all of these oscillators are adjacent to each other, however, we will not concern ourselves with this additional complication herein.

Remark 4: In the present paper we consider only the linear stability of the multibreathers. One may naturally be concerned about the possibility of a stronger form of a stability result. In that light, it could be expected to acquire exponential stability of these solutions like it is proven in [34] for single-site breathers in Klein-Gordon chains with interactions which decrease algebraically with respect to the the lattice site distances. In addition, in [35] in a different context (in a chain of coupled symplectic maps) it is shown numerically, that there exist areas in the phase space around the periodic orbits of the breathers where, if the motion starts inside it, it will remain there for very long times (in computational terms, practically for ever). These facts imply that one could also acquire exponential stability for this kind of systems. On the other hand, special realizations of 1D chains such as the one considered in [36] can enable the proof of asymptotic stability by taking an appropriate solution limit.

3. Klein-Gordon chain with long range interactions

The picture *radically* changes when the chain involves interactions with range longer than mere nearest neighbors. The range parameter r will be used to indicate the interaction length between the oscillators of the chain. So, for the classic nearest neighbor chain the range is $r = 1$ as shown in fig. 1 while for the next nearest neighbor (NNN) chain the range is $r = 2$ as illustrated in fig. 2 etc. The coupling force between the oscillators of the chain is linear and the coupling constants $\varepsilon_i, i = 1 \dots r$ are not, in general, equal.

The Hamiltonian of a 1D KG chain with long range interactions is:

$$H = \sum_{i=-\infty}^{\infty} [\frac{p_i^2}{2} + V(x_i)] + \frac{1}{2} \sum_{i=-\infty}^{\infty} \sum_{j=1}^{r} \varepsilon_j \left(x_i - x_{i+j}\right)^2 \tag{11}$$

which leads to the equations of motion

$$\ddot{x_i} = -V'(x_i) + \sum_{j=1}^{r} \varepsilon_j (x_{i-j} - 2x_i + x_{i+j})$$

3.1. Persistence of multibreathers

Let $\varepsilon_j = k_j \varepsilon$, with $k_1 = 1$, then the Hamiltonian (11) becomes

$$H = H_0 + \varepsilon H_1 = \sum_{i=-\infty}^{\infty} [\frac{p_i^2}{2} + V(x_i)] + \frac{\varepsilon}{2} \sum_{i=-\infty}^{\infty} \sum_{j=1}^{r} k_j \left(x_i - x_{i+j}\right)^2 \tag{12}$$

Now, since the Hamiltonian is written in the form $H = H_0 + \varepsilon H_1$ the persistence conditions (3) can be used. If we consider again $n + 1$ "central" oscillators and $x_i = \sum_{m=0}^{\infty} A_m \cos(m w_i)$, we get for this case

$$\langle H_1 \rangle = -\frac{1}{2} \sum_{m=1}^{\infty} \sum_{j=1}^{r} \sum_{s=1}^{n-j+1} A_m^2 k_j \cos(m \sum_{l=0}^{j-1} \phi_{s+l}). \tag{13}$$

Note that, in the above we considered $r \leqslant n$ since any interaction of oscillators with $r > n$ does not affect the calculations, which are performed in the anti-continuum limit. So, if one considers $r > n$ then for the calculations in this section it would be equivalent to the choice of $r = n$. By differentiating Eq. 13 with respect to ϕ_i we get

$$\frac{\partial \langle H_1 \rangle}{\partial \phi_i} = 0 \Rightarrow \sum_{m=1}^{\infty} \sum_{p=1}^{r} \sum_{s=z_1}^{z_2} m A_m^2 k_p \sin(m \sum_{l=0}^{p-1} \phi_{s+l}) = 0, \tag{14}$$

or, by taking into consideration the definition of (5),

$$\sum_{p=1}^{r} \sum_{s=z_1}^{z_2} k_p M(\sum_{l=0}^{p-1} \phi_{s+l}) = 0, \tag{15}$$

where $z_1 = \max(1, i - p + 1)$ and $z_2 = \begin{cases} i & \text{for} \quad i + p - 1 \leqslant n \\ n - p + 1 & \text{for} \quad i + p - 1 > n \end{cases}$.

Eqs. 13 and 14 (or 15) may be seem cumbersome to handle, they are much easier to use in the concrete examples that will follow in the next sections.

Remark: Note that, in order for the system to "see" the long range interaction, and reveal all the relevant phenomena, one has to consider $n+1$-site breathers, with $n \geqslant r$. If the case of $n < r$ is considered, only the phenomena which correspond to $r = n$ will appear.

3.2. Stability of multibreathers

Since $H = H_0 + \varepsilon H_1$ the methodology described in section 2 can be used in order to determine the linear stability of multibreathers in this case as well. As we have already mentioned the characteristic exponents of the multibreather provided by the persistence conditions (14) are given, to leading order of approximation, by (8), i.e.

$$\sigma_{\pm i} = \pm\sqrt{-\varepsilon\frac{\partial\omega}{\partial J}\chi_{zi}}, \quad i = 1\dots n,$$

where χ_{zi} are the eigenvalues of $\mathbf{Z}$ with

$$\mathbf{Z} = \mathbf{B_1}\cdot\mathbf{L} = \frac{\partial^2\langle H_1\rangle}{\partial\phi_i\partial\phi_j}\cdot\begin{pmatrix} 2 & -1 & 0 & & \\ -1 & 2 & -1 & 0 & \\ & \ddots & \ddots & \ddots & \\ & 0 & -1 & 2 & -1 \\ & & 0 & -1 & 2 \end{pmatrix}, \quad i,j = 1\dots n. \tag{16}$$

For linear stability we need all the characteristic exponents to be purely imaginary. So, if $P = \varepsilon\frac{\partial\omega}{\partial J} < 0$ we need all the eigenvalues of $\mathbf{Z}$ to be negative, while if $P = \varepsilon\frac{\partial\omega}{\partial J} > 0$ we need all the eigenvalues of $\mathbf{Z}$ to be positive.

As it has been already mentioned the form of the matrix $\mathbf{L}$ remains the same as in (10) but the form of $\mathbf{B_1}$ varies for different values of the range r.

Without loss of generality we can consider $i \leqslant j$, since the $\mathbf{B_1}$ matrix is symmetric. Let $d = j - i + 1$, then the general form of $\frac{\partial^2\langle H_1\rangle}{\partial\phi_i\partial\phi_j}$ is

$$\frac{\partial^2\langle H_1\rangle}{\partial\phi_i\partial\phi_j} = \begin{cases} 0 & \text{if} \quad d > r \\ \dfrac{1}{2}\displaystyle\sum_{m=1}^{\infty}\sum_{p=d}^{r}\sum_{s=z_1}^{z_2} m^2 A_m^2 k_p \cos(m\sum_{l=0}^{p-1}\phi_{s+l}) & \text{if} \quad d \leqslant r \end{cases}, \tag{17}$$

or, by taking under consideration the definition of (9),

$$\frac{\partial^2\langle H_1\rangle}{\partial\phi_i\partial\phi_j} = \begin{cases} 0 & \text{if} \quad d > r \\ \displaystyle\sum_{p=d}^{r}\sum_{s=z_1}^{z_2} k_p f(\sum_{l=0}^{p-1}\phi_{s+l}) & \text{if} \quad d \leqslant r \end{cases}. \tag{18}$$

Now z_1 is given by $z_1 = \max(1, i-p+d)$, while z_2 is still given by $z_2 = \begin{cases} i & \text{for} \quad i+p-1 \leqslant n \\ n-p+1 & \text{for} \quad i+p-1 > n \end{cases}$.

We cannot formulate a general theorem like Theorem 1 in the case on lattices with $r > 1$ since the sign of the eigenvalues of $\mathbf{Z}$ depends on the number of the roots the persistence conditions have. As long as there exist only standard multibreathers the situation is described by Theorem 1. But, when phase-shift breathers emerge the situation changes and we cannot a priori determine the sign of χ_z's. In that light a theorem analogous to Theorem 1 appears unlikely in a general setting.

In order to demonstrate the use of the results of this section, in what follows, we will examine some particular cases.

4. 3-site breathers with $r = 2$

4.1. The $\varepsilon_1 = \varepsilon_2 = \varepsilon$ case

4.1.1. Persistence of multibreathers

The simplest case to check the effect of long range interactions is the one of 3 central oscilators (i.e. $n = 2$) and range $r = 2$. As we have already mentioned, any range $r > 2$ would not affect our calculations. First we will check the case $k_1 = k_2 = 1 \Rightarrow \varepsilon_1 = \varepsilon_2 = \varepsilon$.

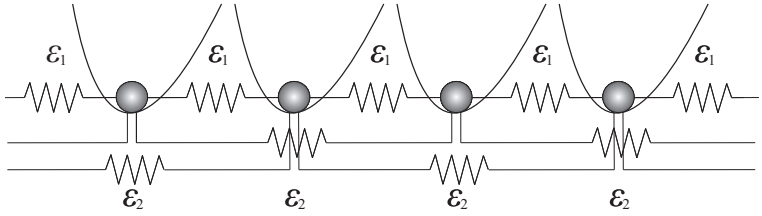

Figure 2: The $r = 2$ Klein-Gordon chain with next nearest neighbor interactions

In this case the Hamiltonian (12) reads

$$H = H_0 + \varepsilon H_1 = \sum_{i=-\infty}^{\infty} \frac{1}{2} p_i^2 + V(x_i) + \frac{\varepsilon}{2} \sum_{i=-\infty}^{\infty} \left[(x_i - x_{i+1})^2 + (x_i - x_{i+2})^2 \right].$$

Since we consider a 3-site breather, H_1 becomes at the anti-continuum limit

$$H_1 = x_1^2 + x_2^2 + x_3^2 + (x_1 - x_2)^2 + (x_1 - x_3)^2 + (x_2 - x_3)^2$$

and

$$\langle H_1 \rangle = -\frac{1}{2} \sum_{m=1}^{\infty} A_m^2 \left\{ \cos(m\phi_1) + \cos(m\phi_2) + \cos[m(\phi_1 + \phi_2)] \right\},$$

according also to (13), for $n = 2$ and $r = 2$. The persistence conditions (14) become

$$\frac{\partial \langle H_1 \rangle}{\partial \phi_i} = 0 \Rightarrow \sum_{m=1}^{\infty} m A_m^2 \left\{ \sin(m\phi_i) + \sin[m(\phi_1 + \phi_2)] \right\} = 0, \quad \text{for} \quad i = 1, 2 \tag{19}$$

or, by taking into consideration the definition of $M(\phi)$ in (5),

$$M(\phi_i) + M(\phi_1 + \phi_2) = 0, \quad \text{for} \quad i = 1, 2. \tag{20}$$

This equation, in addition to the standard solutions

$$\phi_i = 0, \pi,$$

provides also the solutions

$$\phi_1 = \phi_2 = 2\pi/3, \phi_1 = \phi_2 = 4\pi/3.$$

The multibreather solutions with $\phi_i \neq 0$ are called *phase-shift multibreathers* or phase-shift breathers. The anti-phase and phase-shift configurations are depicted in figs. 3 and 4. For a better visualization one can also refer to videos 1 and 2 [supplementary files 1 and 2 here] (video 3 shows an in-phase configuration [supplementary file 3 here]).

In order to produce these figures (and videos) we used the on-site potential $V(x) = \frac{x^2}{2} - 0.15\frac{x^3}{3} - 0.05\frac{x^4}{4}$ and initial conditions which correspond to motion with period $T = 7$ and frequency $\omega = 2\pi/T = 2\pi/7 \simeq 0.8976$. The same potential is used for every numerical calculation throughout this work, although it is straightforward to apply the relevant notions to arbitrary potentials of the Klein-Gordon type.

Remark 1: The persistence conditions (20) provide 2 equations.

$$\begin{aligned} M(\phi_1) + M(\phi_1 + \phi_2) &= 0 \\ M(\phi_2) + M(\phi_1 + \phi_2) &= 0. \end{aligned} \tag{21}$$

By substraction of equations (21) we get

$$M(\phi_1) = M(\phi_2) \tag{22}$$

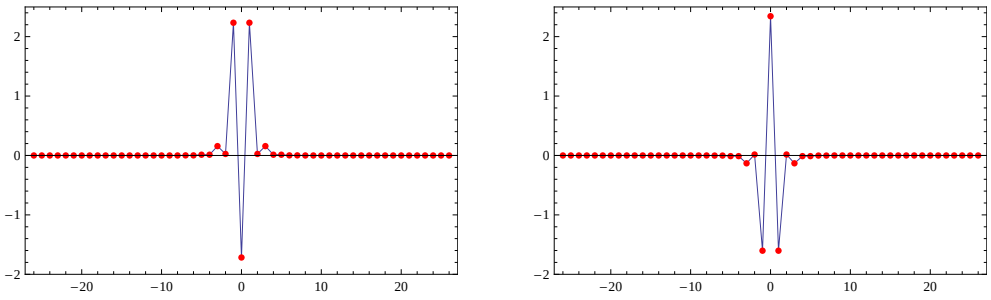

Figure 3: [Color online] Two snapshots of a 3-site ($n = 2$), anti-phase ($\phi_1 = \phi_2 = \pi$) multibreather in a range $r = 2$ Klein-Gordon chain with $\varepsilon_1 = \varepsilon_2 = 0.02$ and frequency $\omega = 2\pi/7$. See also video 1 [supplementary file 1].

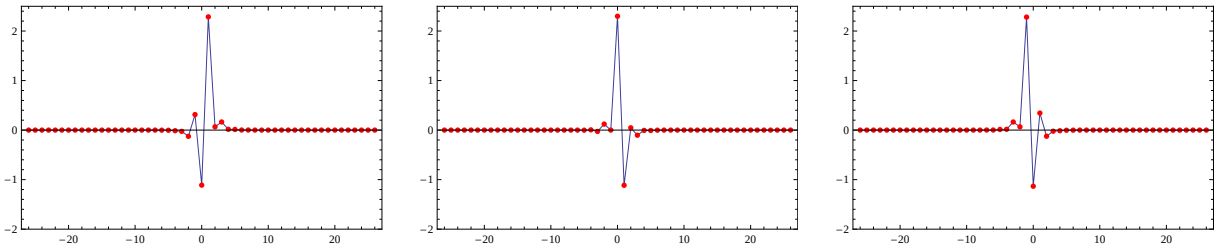

Figure 4: [Color online] Three snapshots of a 3-site ($n = 2$), phase-shift ($\phi_1 = \phi_2 \neq 0, \pi$) multibreather in a range $r = 2$ Klein-Gordon chain with $\varepsilon_1 = \varepsilon_2 = 0.02$ and frequency $\omega = 2\pi/7$. See also video 2 [supplementary file 2 here].

which has, besides the trivial solutions $\phi_i = 0, \pi$, two other obvious solutions: $\phi_1 = \phi_2$ and $\phi_1 + \phi_2 = \pi$ for $0 \leqslant \phi_i \leqslant 2\pi$. The last solution does not provide any new information because by substituting this into equations (21) we get $M(\phi_1) = M(\phi_2) = 0$, which , as it is shown in [25], only possesses the $\phi_i = 0, \pi$ solutions. But the $\phi_1 = \phi_2 = \phi$ solution can reduce the two equations (21) into equation (23)

$$M(\phi) + M(2\phi) = 0. \tag{23}$$

Remark 2: Our numerical computations strongly suggest that for all the phase-shift solutions it is $\phi_1 = \phi_2$, yet a rigorous proof of this fact is still an open problem. So, equation (23) can be used in order to calculate all the solutions of the persistence conditions (20), except for the mixed one $\{\phi_1 = 0,\ \phi_2 = \pi\}$ (or equivalently $\{\phi_1 = \pi,\ \phi_2 = 0\}$).

Remark 3: In the case under consideration ($n = 2$, $r = 2$, $k_i = 1$), all the available solutions correspond to ϕ_i's which make each of the terms of the sum vanish in (19) which obviously provides a zero total.
Remark 4: The case under consideration is equivalent to the 3-site breathers on a hexagonal lattice which has already been studied in [31, 37]. It can be effectively considered as a one-dimensional realization of such a lattice. In that context, the phase-shift multibreathers can be alternatively thought as "discrete vortices", as they are solutions which complete a phase rotation by 2π, as one traverses a discrete contour (which consists of the relevant triangle of sites).
Remark 5: As an aside, it should be mentioned that an additional motivation for the consideration of such next-nearest neighbor interactions stems from the consideration of zigzag arrays, similar to the waveguide arrays proposed theoretically in the context of nonlinear optics (and hence in the realm of the DNLS equation) in [38].
Remark 6: The stability of the above mentioned breathers will be discussed at the end of the next section as a special case of the more general unequal coupling one.

4.2. The $\varepsilon_1 \neq \varepsilon_2$ case

4.2.1. Persistence of multibreathers

Although the $\varepsilon_1 = \varepsilon_2$ case is the easiest and allows us to perform some analytic calculations as well, the natural consideration for the case of next-nearest neighbors is the one with $\varepsilon_1 \neq \varepsilon_2$. Intuitive physical considerations suggest to enforce $\varepsilon_1 \geqslant \varepsilon_2$ (considering coupling force decreasing with the distance between the oscillators) but there are configurations (like the zigzag one) which may also justify settings with $\varepsilon_1 < \varepsilon_2$ [38]. Let $k_1 = 1$ and $k_2 = k$ or, $\varepsilon_1 = \varepsilon$ and $\varepsilon_2 = k\varepsilon$. In this case, the Hamiltonian (12) reads

$$H = H_0 + \varepsilon H_1 = \sum_{i=-\infty}^{\infty} \frac{1}{2} p_i^2 + V(x_i) + \frac{\varepsilon}{2} \sum_{i=-\infty}^{\infty} \left[(x_i - x_{i-1})^2 + k(x_i - x_{i-2})^2 \right].$$

Since we consider a 3-site breather ($n = 2$) we have only two independent ϕ_i's in the anti-continuum limit and by (13) we get

$$\langle H_1 \rangle = -\frac{1}{2} \sum_{m=1}^{\infty} A_m^2 \left\{ \cos(m\phi_1) + \cos(m\phi_2) + k \cos[m(\phi_1 + \phi_2)] \right\}.$$

This leads to the persistence conditions:

$$\frac{\partial \langle H_1 \rangle}{\partial \phi_i} = 0 \Rightarrow \sum_{m=1}^{\infty} m A_m^2 \left\{ \sin(m\phi_i) + k \sin[m(\phi_1 + \phi_2)] \right\} = 0 \equiv M(\phi_i) + kM(\phi_1 + \phi_2) = 0 \quad \text{for} \quad i = 1, 2. \tag{24}$$

Remark: By using the same arguments as in the previous section, if we consider $\phi_1 = \phi_2$, we get from (24),

$$\sum_{m=1}^{\infty} m A_m^2 \left[\sin(m\phi) + k \sin(2m\phi) \right] = 0 \equiv M(\phi) + kM(2\phi) = 0. \tag{25}$$

So, one could use (25) instead of (24) as the relevant persistence condition in order to calculate all the solutions of (24) except of the mixed one $\{\phi_1 = 0,\ \phi_2 = \pi\}$ (or equivalently $\{\phi_1 = \pi,\ \phi_2 = 0\}$).

In the $k = 1$ ($\varepsilon_1 = \varepsilon_2$) case, one could make a choice of $\phi_1 = \phi_2 = 2\pi/3$ or $4\pi/3$ in order to have $\{\sin(m\phi_i) + \sin[m(\phi_1 + \phi_2)]\} = 0\ \forall m$, so that the total sum in (19) would vanish also. This is not possible in the $k \neq 1$ case. So, one may be led to believe that this is an isolated solution and that possibly there are no other solutions than $\phi = 0$ and $\phi = \pi$ in this case. However, it instead turns out that there can be other solutions also which can be calculated numerically for $k \neq 1$. In fact, there is a critical value $k_{cr} = 0.48286$ of k where a pitchfork bifurcation occurs (fig. 5). For values $k < k_{cr}$ the only solutions Eq. (24) [or (25)] has are the trivial ones $\phi_i = 0, \pi$. For $k > k_{cr}$, i.e., past the supercritical pitchfork bifurcation point, other solutions appear with $\phi_i \neq 0, \pi$ (phase-shift breathers) as is shown in fig. 5.

The bifurcation curve has been calculated in two ways. Firstly by numerically modeling the full system and secondly by numerically solving the transcendental existence conditions (24) using a small value of $\varepsilon = 0.001$. The two curves practically coincide, which illustrates the remarkable accuracy of the theory in the vicinity of the anti-continuum limit.

A phase-shift breather with $k = 0.54$ is depicted in fig. 7. For a better visualization of this breather one can also see video 4 [supplementary file 4 here].

It should be noted here that it is worthwhile to examine separately the dynamics ensuing from the above bifurcation and the evolution of the system along its unstable eigendirections. While this is a subject meriting detailed investigation in its own right, we point out here that the expectation is that the dynamics of the newly unstable branches will revolve around the stable (center) branches that emerge from the bifurcation.

4.2.2. Stability of multibreathers

By using the previously developed theory, we can calculate the characteristic exponents of the various configurations of 3-breathers in this lattice setting. The characteristic exponents of the specific solutions are given to first order of approximation by (8) as

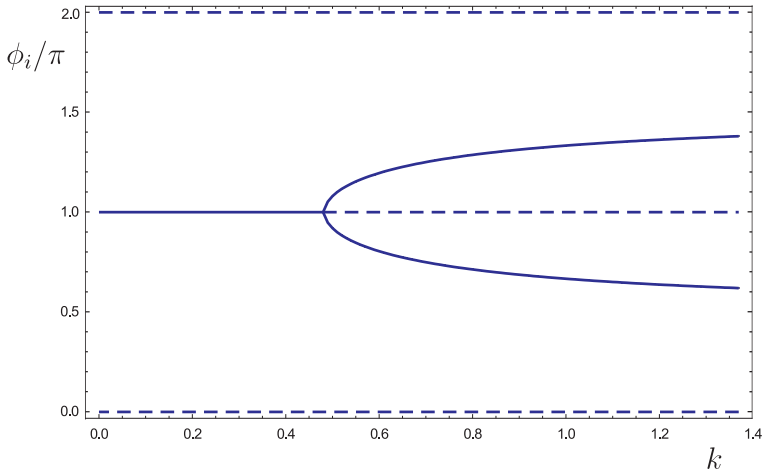

Figure 5: [Color online] The bifurcation diagram for a 3-site ($n = 2$) breather in a $r = 2$ Klein-Gordon chain with $k = \varepsilon_2/\varepsilon_1$. A pitchfork bifurcation occurs for $k = k_{cr} = 0.48286$. The curve is calculated using two methods. The first method is to use the full model, calculate the multibreather solutions with $\varepsilon = 0.001$ and depict them as well as their stability. The second method is to solve numerically (24) and check when solutions with $\phi_i \neq 0, \pi$ appear. The curves produced with the two methods practically coincide (i.e., no difference is discernible at the scale of the plot). The various families that appear here are depicted in more detail in Fig. 6.

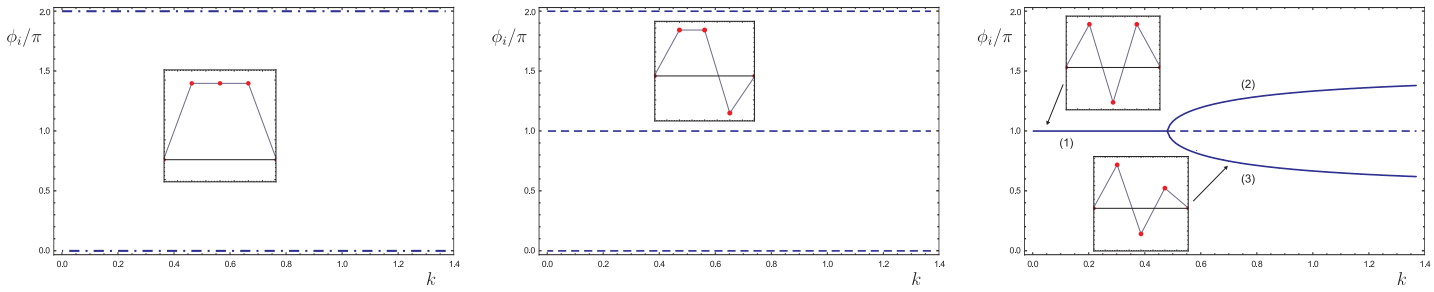

Figure 6: [Color online] The various families that constitute Fig. 5 are depicted. Portraits of the configuration of the central oscillators for the different multibreather families are shown as insets in the corresponding diagrams. The line type in the figures depend in the number of positive χ_z (equivalently, the number of real eigenvalue pairs for $P \equiv \varepsilon \dfrac{\partial \omega}{\partial J} < 0$) the corresponding family possesses: no positive χ_z corresponds to solid line, 1 positive χ_z corresponds to dashed line and 2 to dashed-dotted line. In **(a)** the in-phase configuration is depicted $\{\phi_1 = \phi_2 = 0 \text{ (or } 2\pi)\}$ which possesses 2 positive χ_z. In **(b)** the mixed configuration is shown $\{\phi_1 = 0,\ \phi_2 = \pi\}$ which possesses 1 positive and 1 negative χ_z. In **(c)** two families are shown. The first is the anti-phase one $\{\phi_1 = \phi_2 = \pi\}$. It has 2 negative χ_z until $k < k_{cr} = 0.48286$ while it has 1 positive and 1 negative χ_z for $k > k_{cr}$. At this point the anti-phase family bifurcates to provide the phase-shift configuration $\{\phi_1 = \phi_2 \neq 0, \pi\}$. This family is represented by $\phi_1 = \phi_2 = (2)$ or $\phi_1 = \phi_2 = (3)$ and has no positive (2 negative) χ_z. All of these together are depicted in Fig. 5. When two line segments coincide the more dense is shown.

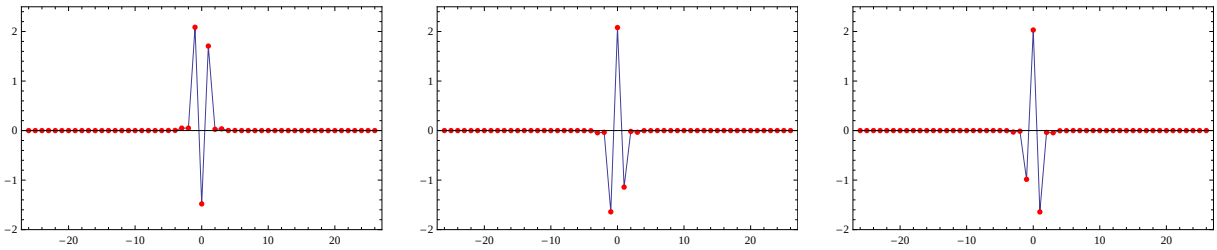

Figure 7: [Color online] Snapshots of a phase-shift 3-site breather for $\varepsilon_1 = 0.02$ and $\varepsilon_2 = k_2\varepsilon_1 = 0.56\varepsilon_1$ and frequency $\omega = 2\pi/7$. See also video 4 [supplementary file 4 here].

$$\sigma_{\pm i} = \pm\sqrt{-\varepsilon\frac{\partial\omega}{\partial J}\chi_{zi}},$$

where χ_{zi} are the eigenvalues of the matrix $\mathbf{Z}$ defined in (16).

In the case under consideration of 3-site ($n = 2$) breathers with range $r = 2$ we have, also from (18),

$$\frac{\partial^2\langle H_1\rangle}{\partial\phi_i\partial\phi_j} = \begin{pmatrix} f(\phi_1) + kf(\phi_1+\phi_2) & kf(\phi_1+\phi_2) \\ kf(\phi_1+\phi_2) & f(\phi_2) + kf(\phi_1+\phi_2) \end{pmatrix} \quad \text{and} \quad \mathbf{L} = \begin{pmatrix} 2 & -1 \\ -1 & 2 \end{pmatrix}.$$

So, we get from (16),

$$\mathbf{Z} = \frac{\partial^2\langle H_1\rangle}{\partial\phi_i\partial\phi_j}\cdot\mathbf{L} = \begin{pmatrix} 2f_1 + kf_{1+2} & kf_{1+2} - f_1 \\ kf_{1+2} - f_2 & 2f_2 + kf_{1+2} \end{pmatrix},$$

where the function $f(\phi)$ is defined as in (9), and $f_{1+2} \equiv f(\phi_1+\phi_2)$, while $f_i = f(\phi_i)$ for $i = 1, 2$.

For linear stability it is required that all of the characteristic exponents be purely imaginary. So, the stability is determined by the sign of χ_{zi}.

In particular, we check the configurations that can appear in this case.

- $\phi_1 = \phi_2$. This is the general case and includes the in-phase $\{\phi_1 = \phi_2 = 0\}$, the out-of-phase $\{\phi_1 = \phi_2 = \pi\}$ and phase-shift configurations $\{\phi_1 = \phi_2 \neq 0, \pi\}$. The corresponding eigenvalues χ_z are $\chi_{z1} = 3f_\phi$ and $\chi_{z2} = f_\phi + 2kf_{2\phi}$.

- $\phi_1 = 0, \phi_2 = \pi$. This is the only solution with $\phi_1 \neq \phi_2$. For this case it is $\chi_{z1,2} = f_0 + (1+k)f_\pi \pm \sqrt{f_0^2 - (1+k)f_0f_\pi + f_\pi^2(1-k+k^2)}$.

Remark: We have that $f_0 > 0$ as a direct consequence of the definition (9) of $f(\phi)$. On the other hand it is $f_\pi < 0$. This can be rigorously proven ([20] Lemma 3) but it can also be intuitively understood by the definition (9) of $f(\phi)$ and the fact that the first term of the Fourier expansion of $x(w)$ (4) is the dominant one. Using the same arguments we can conclude that $|f_0| > |f_\pi|$. So, we can immediately conclude that in the in-phase $\{\phi_1 = \phi_2 = 0\}$ configuration it is $\chi_{zi} > 0$, while in the mixed $\{\phi_1 = 0,\ \phi_2 = \pi\}$ configuration it is $\chi_{z1} > 0$, $\chi_{z2} < 0$.

On the other hand for the anti-phase $\{\phi_1 = \phi_2 = \pi\}$ configuration, the formulas for the χ_{zi} read

$$\chi_{z1} = 3f_\pi \quad \text{and} \quad \chi_{z2} = f_\pi + 2kf_0. \tag{26}$$

The χ_{z1} eigenvalue is always negative while the sign of the χ_{z2} depends on the value of k. This can provide us with a criterion about the value of k_{cr} where the bifurcation occurs, since, at this point χ_{z2} changes sign. So, by (26) we get $\chi_{z2} = 0 \Rightarrow k_{cr} = -\dfrac{f_\pi}{2f_0}$.

The values of f_0 and f_π depend on the particular on-site potential as well as on the frequency we examine, so, the value k_{cr} is not fixed. But, if we consider breathers with relatively low amplitude, which amounts to the breather frequency ω being close to the phonon frequency ω_p, a rough estimation of k_{cr} can be made. In such a case, the nonlinear character of the system is not fully revealed yet which means that the A_1 term in the development (4) is by far the most dominant one. This results to $|f_0| \simeq |f_\pi|$ and consequently $k_{cr} \simeq 0.5$.

In order to check our estimation, we perform some numerical calculations for the lattice with potential $V(x) = \frac{x^2}{2} - 0.15\frac{x^3}{3} - 0.05\frac{x^4}{4}$ which we use throughout this work, considering a motion with $\omega = 2\pi/7 \simeq 0.8976$. For this frequency, it is $|f_0/f_\pi| \simeq 1$, as can be seen in Fig. 8, so our estimation holds. In particular, it is $f_\pi = -1.48658$, $f_0 = 1.53934$ and $k_{cr} = -\frac{f_\pi}{2f_0} = 0.48286$, which is precisely the value where the bifurcation occurs, while being very close also to the rough estimation (of 0.5) above. Note that, as it can be seen in Fig. 8, if we had chosen a smaller breather frequency ω, our estimation would be completely mistaken, since for small values of ω it is $|f_0/f_\pi| > 1$.

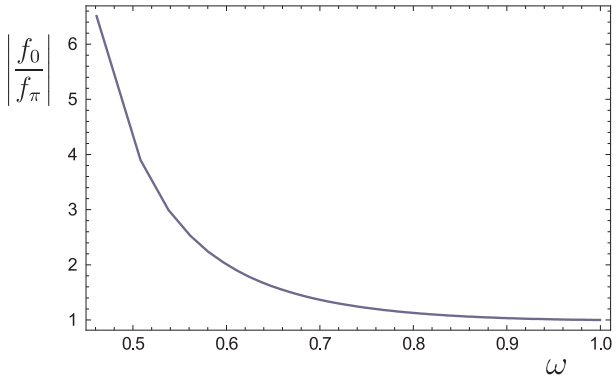

Figure 8: [Color online] Dependence of the $|f_0/f_\pi|$ ratio with respect to the frequency ω of the breather.

Remarks about figs. 5 and 6: In figs. 5 and 6 all the multibreather families that exist in the present configuration ($n = 2$, $r = 2$) are shown. The multibreather families correspond to solution families of Eqs. 24. These families are categorized by the phase differences ϕ_i between the successive oscillators in the anticontinuous limit. The values of ϕ_i in the usual families ($\phi_i = 0, \pi$) are constant with increasing k, while in the phase-shift ($\phi_i \neq 0, \pi$) families their values change with respect to k.

The various solution families are represented by various line (or curve) segments in the figures. The kind of the line depends on the number of positive χ_z (i.e., of real eigenvalue pairs for $P \equiv \varepsilon\frac{\partial\omega}{\partial J} < 0$) that the corresponding solution has. So, for no $\chi_z > 0$ we use a solid line, for one $\chi_z > 0$ we use a dashed line while for two $\chi_z > 0$ we use a dashed-dotted line. Since in Fig. 5 some of the families coincide, we separated the information in this figure into 3 panels in Fig. 6. These 3 panels together compose Fig. 5. If the segments which represent two or more distinct families of solutions coincide, the more dense is shown in the figure. In order to facilitate the visualization of the various families, we added insets in Figs. 6 demonstrating the profiles of (and hence illustrating the phase difference between) the central oscillators in the anticontinuum limit. This has as a result only solid and dashed segments to appear in Fig. 5. The families that are depicted in the figure are:

- $\{\phi_1 = \phi_2 = 0$ (or $2\pi)\}$ (in-phase). This family is shown in Fig. 6(a) and possesses 2 positive χ_z.
- $\{\phi_1 = 0$ or π, $\phi_2 = \pi\}$ (mixed). This family is depicted in Fig. 6(b) and possesses 1 positive and 1 negative χ_z.
- $\{\phi_1 = \phi_2 = \pi\}$ (anti-phase). It is represented in Fig. 6(c) by $\phi_1 = \phi_2 = (1)$. It has no positive χ_z until $k < k_{cr}$ while it has 1 positive and 1 negative χ_z for $k > k_{cr}$. At this point the $\phi_1 = \phi_2 = \pi$ family becomes subject to the bifurcation that gives rise to phase-shift multibreathers.

- $\phi_1 = \phi_2 \neq 0, \pi$ (phase-shift). This family is represented in Fig. 6(c) by $\phi_1 = \phi_2 = (2)$ or $\phi_1 = \phi_2 = (3)$ and has no positive χ_z.

Since the stability of the multibreathers is also determined by the sign of $P \equiv \varepsilon \dfrac{\partial \omega}{\partial J}$, the above are summarized, in terms of stability of the solutions, in Table 1.

	P	k	In-phase $\phi_1 = \phi_2 = 0$	Out-of-phase $\phi_1 = \phi_2 = \pi$	Phase-shift $\phi_1 = \phi_2 \neq 0, \pi$
Linear Stability	$P < 0$	$k < k_{cr}$	unstable	stable	–
	$P < 0$	$k > k_{cr}$	unstable	unstable	stable
	$P > 0$	$k < k_{cr}$	stable	unstable	–
	$P > 0$	$k > k_{cr}$	stable	unstable	unstable

Table 1: [Color online] Stability of the various $n = 2$, $r = 2$, breather configurations depending on the values of $P \equiv \frac{\partial \omega}{\partial J}$ and k. With the dash we denote that this particular family does not exist for this range of values of k.

Stability of the various 3-site breather configurations in the $\varepsilon_1 = \varepsilon_2$ case: Using the above derived results we can conclude what it is already known from [31, 37]. i.e. for $P < 0$, as long as $k < k_{cr}$ the only stable configuration is the anti-phase one, while for $k > k_{cr}$ the stable configuration is the phase-shift one (which corresponds in this case to the "vortex" configuration of [31, 37]). On the other hand for $P > 0$ the only stable configuration is the in-phase one.

5. 4-site breathers with $r = 2$

In the next configuration we will consider four central oscillators, in order to study larger configurations, but we will keep the range to $r = 2$ as a first step.

5.1. Persistence of multibreathers

We will treat the two cases $\varepsilon_1 = \varepsilon_2$ and $\varepsilon_1 \neq \varepsilon_2$ together, since the latter is a special case of the former with $k_1 = k_2 = 1$. Since we consider 4 ($n = 3$) central oscillators and range $r = 2$, (13) gives for $k_1 = 1$ and $k_2 = k$,

$$\langle H_1 \rangle = -\frac{1}{2} \sum_{m=1}^{\infty} A_m^2 \{\cos(m\phi_1) + \cos(m\phi_2) + \cos(m\phi_3) + \\ + k \cos[m(\phi_1 + \phi_2)] + k \cos[m(\phi_2 + \phi_3)]\}$$

while, the corresponding persistence conditions (14) become

$$\begin{aligned} M(\phi_1) + k\, M(\phi_1 + \phi_2) &= 0 \\ M(\phi_2) + k\, [M(\phi_1 + \phi_2) + M(\phi_2 + \phi_3)] &= 0 \\ M(\phi_3) + k\, M(\phi_2 + \phi_3) &= 0 \end{aligned}$$

which have the trivial solutions $\phi_i = 0, \pi$, as well as non trivial ones, as can be seen in fig. 9.

By using the same arguments as in the previous section, which are also verified by our numerical investigation we have that for all the phase-shift breathers it is $\phi_1 = \phi_3$. At $k = k_{cr}^{(1)} = 0.3219$ the anti-phase $\{\phi_1 = \phi_2 = \phi_3 = \pi\}$ family becomes subject to a bifurcation that generates the phase-shift 4-site breathers. We should also note in passing (see details below) that, in addition to this supercritical pitchfork, the figure reveals also a sub-critical pitchfork bifurcation that terminates the two asymmetric branches upon their collision with the branch with the mixed family $\{\phi_1 = \phi_3 = \pi,\ \phi_2 = 0\}$ at $k_{cr}^{(2)} = 1.0736$.

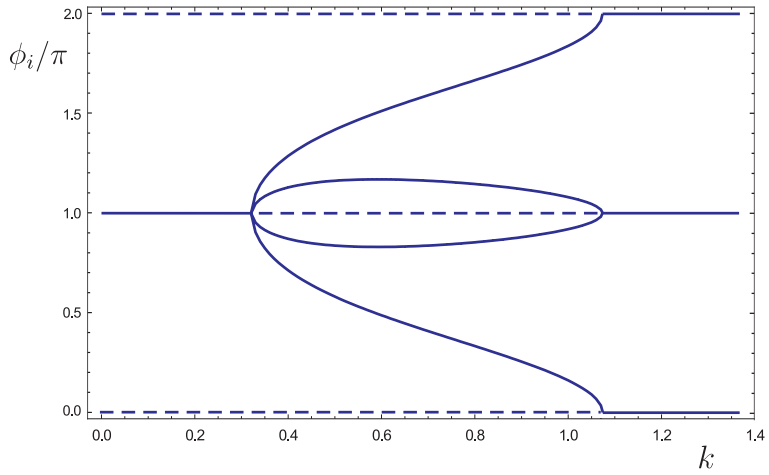

Figure 9: [Color online] In this diagram all the existing families of 4-site ($n = 3$) breathers in a KG chain with range $r = 2$ are depicted. For a more detailed view of the particular families appearing in this diagram, refer also to fig. 10.

5.2. Stability of multibreathers

The stability of the existing multibreather solutions can be calculated by using the previously developed theory. Their corresponding characteristic exponents are given to first order of approximation by (8). In the case under consideration of 4-site ($n = 3$) breathers with range $r = 2$ we have from (17)

$$\frac{\partial^2\langle H_1\rangle}{\partial\phi_i\partial\phi_j} = \begin{pmatrix} f_1 + k\,f_{1+2} & k\,f_{1+2} & 0 \\ k\,f_{1+2} & f_2 + k\,f_{1+2} + k\,f_{2+3} & k\,f_{2+3} \\ 0 & k\,f_{2+3} & f_3 + k\,f_{2+3} \end{pmatrix} \quad \text{and} \quad \mathbf{L} = \begin{pmatrix} 2 & -1 & 0 \\ -1 & 2 & -1 \\ 0 & -1 & 2 \end{pmatrix}$$

So, (16) gives

$$\mathbf{Z} = \frac{\partial^2\langle H_1\rangle}{\partial\phi_i\partial\phi_j}\cdot\mathbf{L} = \begin{pmatrix} 2f_1 + kf_{1+2} & kf_{1+2} - f_1 & -kf_{1+2} \\ k(f_{1+2} - f_{2+3}) - f_2 & 2f_2 + k(f_{1+2} + f_{2+3}) & k(f_{2+3} - f_{1+2}) - f_2 \\ -kf_{2+3} & kf_{2+3} - f_3 & 2f_3 + kf_{2+3} \end{pmatrix}$$

For the general case $\phi_1 = \phi_3$, the eigenvalues of $\mathbf{Z}$ are

$$\chi_{z1} = 2(f_1 + kf_{1+2}) \quad \text{and} \quad \chi_{z2,3} = f_1 + f_2 + kf_{1+2} \pm \sqrt{f_1^2 + f_2^2 - 2kf_1f_{1+2} + k^2f_{1+2}^2}.$$

The only configurations that are not included in the case above are the mixed ones $\{\phi_1 = \phi_2 = 0,\ \phi_3 = \pi\}$ and $\{\phi_1 = \phi_2 = \pi,\ \phi_3 = 0\}$, which both have 2 positive χ_z, independently of the value of k.

Remark: The χ_{z2} eigenvalues of the anti-phase and mixed configurations can be used in order to calculate the values of $k_{cr}^{(1)}$ and $k_{cr}^{(2)}$. The χ_{z2} for the anti-phase configuration is

$$\chi_{z2} = 2f_\pi + kf_0 + \sqrt{2f_\pi^2 - 2kf_\pi f_0 + k^2f_0^2}.$$

Since for $k = k_{cr}^{(1)}$ it is $\chi_{z2} = 0$ we get $k_{cr}^{(1)} = -\dfrac{f_\pi}{3f_0} \simeq \dfrac{1}{3}$. The last rough estimation can be performed only when we consider breathers with frequency ω close to the phonon frequency ω_p (see also the discussion in the previous section), where $|f_0| \simeq |f_\pi|$. In order to be more precise, for the potential and frequency used in the present work, we get $k_{cr} = 0.3219$.

On the other hand, the χ_{z2} eigenvalue for the mixed $\{\phi_1 = \phi_3 = \pi,\ \phi_2 = 0\}$ configuration is

$$\chi_{z2} = f_0 + (1 + k)f_\pi + \sqrt{(1 - k)^2f_\pi^2 + f_0}.$$

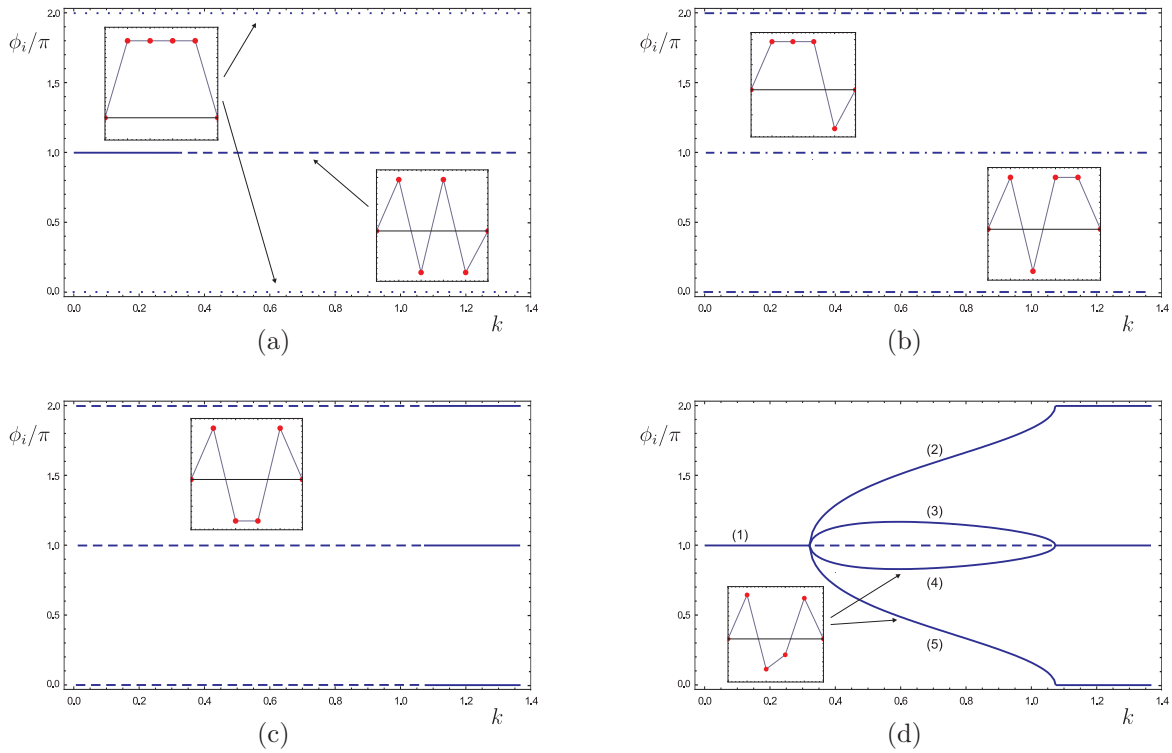

Figure 10: [Color online] The various families that appear in Fig. 9 are depicted. Portraits of the configuration of the central oscillators for the different multibreather families are shown as insets in the corresponding diagrams. The line (or curve) type in the figures depends on the number of positive χ_z that the corresponding family possesses: no positive χ_z corresponds to a solid line, 1 positive χ_z corresponds to a dashed line, 2 to a dash-dotted and 3 to a dotted line. In **(a)** two multibreather families are depicted. The first is the in-phase one with $\{\phi_1 = \phi_2 = \phi_3 = 0 \text{ (or } 2\pi)\}$ which possesses 3 positive χ_z. The second one is the anti-phase one with $\{\phi_1 = \phi_2 = \phi_3 = \pi\}$. It has no positive χ_z until $k < k_{cr}^{(1)} = 0.3219$ while it has 1 positive χ_z for $k > k_{cr}^{(1)}$. At this point the anti-phase family gives rise, through a supercritical pitchfork, to the the phase-shift $\{\phi_1 = \phi_2 \neq 0, \pi\}$ family. In **(b)** the mixed 1 configuration is shown $\{\phi_1 = \phi_2 = 0 \text{ or } 2\pi,\ \phi_3 = \pi\}$ or $\{\phi_1 = \phi_2 = \pi, \phi_3 = 0 \text{ or } 2\pi\}$. These families possess 2 positive and 1 negative χ_z each. In **(c)** the mixed 2 family $\{\phi_1 = \phi_3 = \pi, \phi_2 = 0 \text{ or } 2\pi\}$ is shown. It possesses 1 positive χ_z for $k < k_{cr}^{(2)} = 1.0736$ and no positive χ_z for $k > k_{cr}^{(2)}$. At this point the mixed 2 family collides with the phase-shift one. In **(d)** the phase-shift $\{\phi_1 = \phi_2 \neq 0, \pi\}$ family is shown and it is represented by $\phi_1 = \phi_3 = (3)$ and $\phi_2 = (2)$ or $\phi_1 = \phi_3 = (4)$ and $\phi_2 = (5)$. It exists for $k_{cr}^{(1)} < k < k_{cr}^{(2)}$. At $k = k_{cr}^{(1)}$ it bifurcates from the anti-phase family, while at $k = k_{cr}^{(2)}$ it emerges with the mixed 2 family, and possesses no positive χ_z. Fig. 9 contains all of the above families together, where, when two line segments coincide the more dense is shown.

Since for $k = k_{cr}^{(2)}$ it is $\chi_{z2} = 0$ we get $k_{cr}^{(2)} = -\dfrac{f_0}{2f\pi + f_0} \simeq 1$ or, for the specific potential and frequency used in this work $k_{cr}^{(2)} = 1.0736$.

Remarks on the stability diagram of Figs. 9 and 10: In Figs. 9 and 10 all the multibreather families they exist in the present configuration ($n = 3$, $r = 2$) are shown. The kind of the line (or curve) used for every segment depends on the number of positive χ_z as follows: no positive $\chi_z \rightarrow$ solid, 1 positive $\chi_z \rightarrow$ dashed, 2 positive $\chi_z \rightarrow$ dashed-dotted, 3 positive $\chi_z \rightarrow$ dotted. All the families shown in Fig.10 are depicted together in Fig.9. Since, if two segments coincide, the more dense is shown, in Fig.9 we can see only solid and dashed segments. The families which are depicted in these two figures are the following:

- $\{\phi_1 = \phi_2 = \phi_3 = 0 \text{ (or } 2\pi)\}$ (in-phase). This family is shown in Fig.10(a) and has 3 positive χ_z.
- $\{\phi_1 = \phi_2 = \phi_3 = \pi\}$ (anti-phase). It is shown in Fig.10(a) and has no positive χ_z for $k < k_{cr}^{(1)} = 0.3219$ while it possesses one positive χ_z for $k > k_{cr}^{(1)}$. At this point the anti-phase family bifurcates to provide

the phase-shift breather family.

- $\{\phi_1 = \phi_2 = 0,\ \phi_3 = \pi\}$ or $\{\phi_1 = \phi_2 = \pi,\ \phi_3 = 0\}$ (mixed 1). These families are depicted in Fig.10(b) and they both possess 2 positive χ_z
- $\{\phi_1 = \phi_3 = \pi,\ \phi_2 = 0\ (\text{or } 2\pi)\}$ (mixed 2). It is shown in Fig.10(c). For $k < k_{cr}^{(2)}$ it has 1 positive χ_z, while for $k > k_{cr}^{(2)}$ it has no positive χ_z. At $k = k_{cr}^{(2)} = 1.0736$, this family collides with the phase-shift family.
- $\phi_1 = \phi_3, \phi_2 \neq 0, \pi$ (phase shift). This family is represented in Fig.10(d) by $\phi_1 = \phi_3$=(3) and ϕ_2=(2) (or $\phi_1 = \phi_3$=(4) and ϕ_2=(5)) and has no positive χ_z. It begins to exist at $k = k_{cr}^{(1)}$ where it bifurcates from the anti-phase family and cease to exist at $k = k_{cr}^{(2)}$ where it collides with the mixed 1 family.

Since the stability of the multibreathers is also determined by the sign of $P \equiv \varepsilon \frac{\partial \omega}{\partial J}$ the above are summarized, in terms of the linear stability of the corresponding configurations, in Table 2.

	P	k	In-phase $\phi_1 = \phi_2 = \phi_3 = 0$	Out-of-phase $\phi_1 = \phi_2 = \phi_3 = \pi$	Phase-shift $\phi_1 = \phi_3, \phi_2 \neq 0, \pi$	Mixed $\phi_1 = \phi_3 = \pi, \phi_2 = 0$
Linear Stability	$P < 0$	$k < k_{cr}^{(1)}$	unstable	stable	–	unstable
	$P < 0$	$k_{cr}^{(1)} < k < k_{cr}^{(2)}$	unstable	unstable	stable	unstable
	$P < 0$	$k > k_{cr}^{(2)}$	unstable	unstable	–	stable
	$P > 0$	$k < k_{cr}^{(1)}$	stable	unstable	–	unstable
	$P > 0$	$k_{cr}^{(1)} < k < k_{cr}^{(2)}$	stable	unstable	unstable	unstable
	$P > 0$	$k > k_{cr}^{(2)}$	stable	unstable	–	unstable

Table 2: [Color online] Stability of the various 4-site ($n = 3$) and range $r = 2$, breather configurations depending on the values of $P \equiv \frac{\partial \omega}{\partial J}$ and k. With the dash we denote that this particular family does not exist for this range of values of k.

6. 4-site breathers with $r = 3$

The natural way to extend our study in 4-site breathers is to consider range of interaction $r = 3$ (i.e., involving interactions with the 3 closest neighbors on each side of the chain), in order for all the central oscillators to interact with each other.

6.1. Persistence of multibreathers

Bearing in mind that $\epsilon_i = \epsilon k_i$ and that $k_1 = 1$, $\langle H_1 \rangle$ in this case becomes

$$\langle H_1 \rangle = -\frac{1}{2} \sum_{m=1}^{\infty} A_m^2 \left\{ \cos(m\phi_1) + \cos(m\phi_2) + \cos(m\phi_3) + \right.$$
$$\left. + k_2 \{ \cos[m(\phi_1 + \phi_2)] + \cos[m(\phi_2 + \phi_3)] \} + k_3 \cos[m(\phi_1 + \phi_2 + \phi_3)] \right\},$$

while the corresponding persistence conditions become

$$M(\phi_1) + k_2 M(\phi_1 + \phi_2) + k_3 M(\phi_1 + \phi_2 + \phi_3) = 0$$

$$M(\phi_2) + k_2 \left[M(\phi_1 + \phi_2) + M(\phi_2 + \phi_3) \right] + k_3 M(\phi_1 + \phi_2 + \phi_3) = 0$$

$$M(\phi_3) + k_2 M(\phi_2 + \phi_3) + k_3 M(\phi_1 + \phi_2 + \phi_3) = 0.$$

For every k_i, there exist the usual $\phi_i = 0, \pi$ solutions, as well as others as it can be seen in fig. 11. By keeping k_3 constant, we get various mono-parametric bifurcation diagrams with k_2 as the parameter. Again, for all the phase shift configurations it is $\phi_1 = \phi_3$. In fig. 11, the bifurcation diagrams for two values of k_3 are depicted, $k_3 = 0.2$ and $k_3 = 0.4$. We see that the value of $k_{2_{cr}}^{(1)}$ where the supercritical bifurcation occurs depends strongly on the value of k_3, while the value of $k_{2_{cr}}^{(2)}$ remains almost constant at $k_{2_{cr}}^{(2)} \simeq 1.075$. The dependence of $k_{2_{cr}}$ with respect to k_3 is shown in fig. 12.

Note that for $k_3 \to 0$ this case coincides with the $r = 2$ case (i.e., the latter is a special case example) and we retrieve the diagram of Fig. 9.

6.2. Stability

As it has already mentioned the stability of the multibreathers is determined by the sign of the eigenvalues $\chi_{z\,i}$, of matrix $\mathbf{Z}$ (16). By (17) we get

$$\frac{\partial^2 \langle H_1 \rangle}{\partial \phi_i \partial \phi_j} = \begin{pmatrix} f_1 + k_2 f_{1+2} + k_3 f_{1+2+3} & k_2 f_{1+2} + k_3 f_{1+2+3} & k_3 f_{1+2+3} \\ k_2 f_{1+2} + k_3 f_{1+2+3} & f_2 + k_2(f_{1+2} + f_{2+3}) + k_3 f_{1+2+3} & k_2 f_{2+3} + k_3 f_{1+2+3} \\ k_3 f_{1+2+3} & k_2 f_{2+3} + k_3 f_{1+2+3} & f_3 + k_2 f_{2+3} + k_3 f_{1+2+3} \end{pmatrix},$$

and since

$$\mathbf{L} = \begin{pmatrix} 2 & -1 & 0 \\ -1 & 2 & -1 \\ 0 & -1 & 2 \end{pmatrix}$$

we finally get

$$\mathbf{Z} = \frac{\partial^2 \langle H_1 \rangle}{\partial \phi_i \partial \phi_j} \cdot \mathbf{L} = \begin{pmatrix} 2f_1 + k_2 f_{1+2} + k_3 f_{1+2+3} & k_2 f_{1+2} - f_1 & k_3 f_{1+2+3} - k_2 f_{1+2} \\ k_2 f_{1+2} + k_3 f_{1+2+3} - f_2 - k_2 f_{2+3} & 2f_2 + k_2(f_{1+2} + f_{2+3}) & k_2 f_{2+3} + k_3 f_{1+2+3} - f_2 - k_2 f_{1+2} \\ k_3 f_{1+2+3} - k_2 f_{2+3} & k_2 f_{2+3} - f_3 & 2f_3 + k_2 f_{2+3} + k_3 f_{1+2+3} \end{pmatrix}.$$

Its eigenvalues are, for $\phi_1 = \phi_3$ and non-specific values of ϕ_i,

$$\chi_{z1} = 2(f_1 + k_2 f_{1+2})$$

$$\chi_{z\,2,3} = f_1 + f_2 + k_2 f_{1+2} + k_3 f_{2\phi_1+\phi_2} \pm \sqrt{f_1^2 + f_2^2 - 2k_2 f_1 f_{1+2} + k_2^2 f_{1+2}^2 - 2k_3 f_2 f_{2\phi_1+\phi_2} + k_3^2 f_{2\phi_1+\phi_2}^2}.$$

Although such analytical formulas exist and accurately predict the stability and bifurcations of the system, a clearer understanding emerges from the observation of the associated bifurcation diagrams (fig. 11). The diagrams present exactly the same solution families as in Fig. 9, but in this case the value of $k_{2_{cr}}^{(1)}$, where the supercritical bifurcation occurs, is strongly affected by the value of k_3, while, the value of $k_{2_{cr}}^{(2)}$, where the subcritical bifurcation occur,s remains almost constant with $k_{2_{cr}}^{(2)} \simeq 1.075$ (Fig. 12). This indicates that, for the range of values of k_3 considered in this figure, the parametric interval of k_2 (the strength of next-nearest neighbor interactions) over which phase-shift solutions exist narrows as k_3 (the strength of interaction with the third-nearest-neighbors) is increased.

7. 4-site breathers in a 2D square lattice with $r = 2$

We now turn our considerations to the case of a square lattice, as the one in Fig. 13, with nearest-neighbor interactions, not only with the horizontal and vertical neighbors, but with the diagonal as well. The latter interaction is assumed to have a strength $\epsilon_2 = k\epsilon_1$ (where $\epsilon_1 \equiv \epsilon$ will be taken to denote the coupling strength of adjacent nodes along the lattice axes). The Hamiltonian for this system is

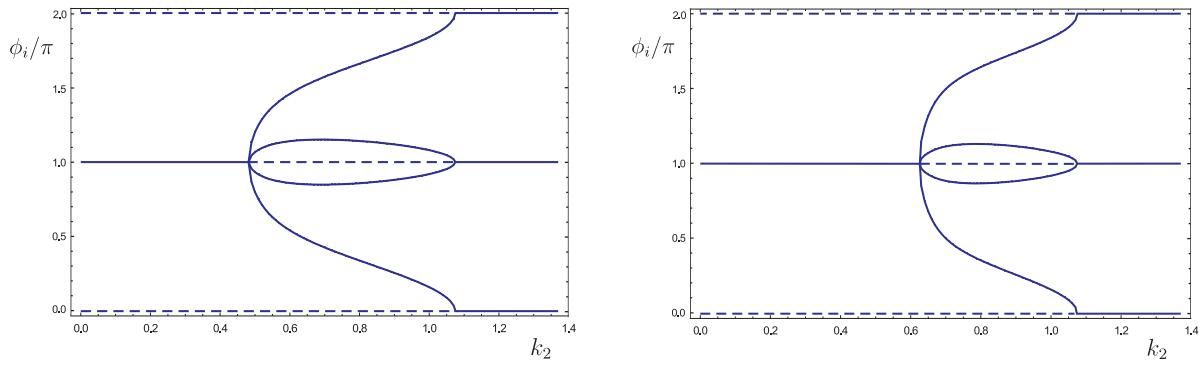

Figure 11: [Color online] In these panels the various 4-site ($n = 3$) multibreathers families in a chain with interaction range $r = 3$ are shown. In the diagram we have considered k_2 variable, while $k_3 = 0.2$ in the left panel and $k_3 = 0.4$ in the right panel. The families depicted are qualitatively the same as the ones in the $n = 3$, $r = 2$ case. The only difference is that in the present case the value of $k_{2cr}^{(1)}$ where the supercritical bifurcation occurs depends strongly on k_3 while the value of $k_{2cr}^{(2)}$ where the subcritical bifurcation occurs remains almost fixed.

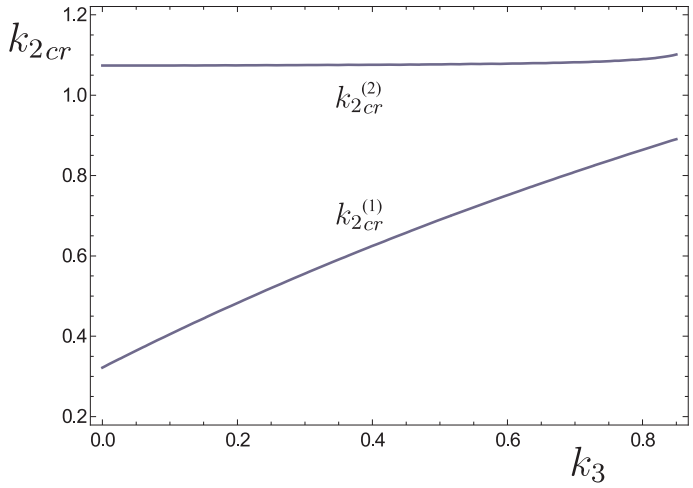

Figure 12: [Color online] The values of the two k_{2cr}, where the bifurcations occur, with respect to k_3. Although $k_{2cr}^{(1)}$ depends strongly on k_3, $k_{2cr}^{(2)}$ remains almost constant at $k_{2cr}^{(2)} \simeq 1.075$.

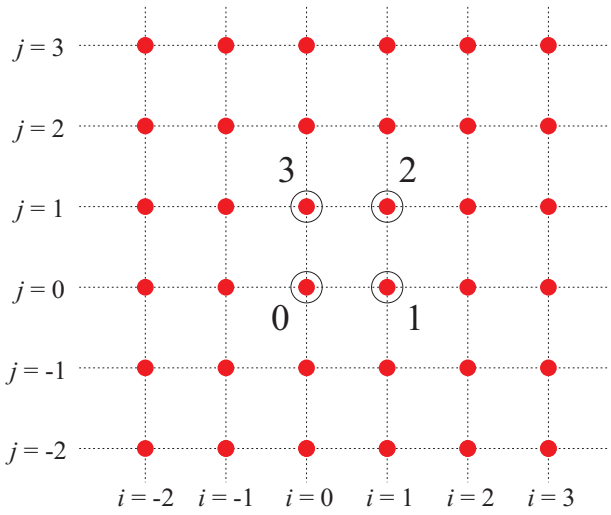

Figure 13: [Color online] In the square lattice under consideration each oscillator is coupled with its neighbour not only in the horizontal and vertical directions but in the diagonal directions as well. So, every lattice site interacts with its 8 neighbours instead of the 4 of the classical KG square lattice configuration. In this setting, we consider 4-site breathers. Let the encircled oscillators in the figure be the central oscillators which are denoted as 0, 1, 2, 3 respectively

$$\begin{aligned} H &= \sum_{i=-\infty}^{\infty}\sum_{j=-\infty}^{\infty}\left[\frac{1}{2}p_{ij}^2+V(x_{ij})\right] \quad +\frac{\varepsilon_1}{2}\sum_{i=-\infty}^{\infty}\sum_{j=-\infty}^{\infty}\left[(x_{ij}-x_{i-1,j})^2+(x_{ij}-x_{i,j-1})^2\right] \\ &\qquad +\frac{\varepsilon_2}{2}\sum_{i=-\infty}^{\infty}\sum_{j=-\infty}^{\infty}\left[(x_{ij}-x_{i-1,j-1})^2+(x_{ij}-x_{i-1,j+1})^2\right] \end{aligned} \tag{27}$$

or

$$\begin{aligned} H = H_0+\varepsilon H_1 \quad &= \sum_{i=-\infty}^{\infty}\sum_{j=-\infty}^{\infty}\left[\frac{1}{2}p_{ij}^2+V(x_{ij})\right]+ \\ &+\frac{\varepsilon}{2}\sum_{i=-\infty}^{\infty}\sum_{j=-\infty}^{\infty}\left\{(x_{ij}-x_{i-1,j})^2+(x_{ij}-x_{i,j-1})^2+k\left[(x_{ij}-x_{i-1,j-1})^2+(x_{ij}-x_{i-1,j+1})^2\right]\right\} \end{aligned} \tag{28}$$

We consider 4 "central" oscillators in the anti-continuum limit and we denote them by 0, 1,2 ,3 as it is shown in fig.13. We have then $\phi_1 = w_1 - w_0$, $\phi_2 = w_2 - w_1$, $\phi_3 = w_3 - w_2$ and $\phi_4 = w_0 - w_3$. But since, by construction, we have $\phi_4 = 2\pi - \phi_1 - \phi_2 - \phi_3$, we have finally only 3 independent ϕ_i's. The $\langle H_1\rangle$ in this case is

$$\begin{aligned} \langle H_1\rangle = -\frac{1}{2}\sum_{m=1}^{\infty} A_m^2 \{&\cos(m\phi_1)+\cos(m\phi_2)+\cos(m\phi_3)+\cos[m(\phi_1+\phi_2+\phi_3)] \\ &+k\{\cos[m(\phi_1+\phi_2)]+\cos[m(\phi_2+\phi_3)]\}\} \end{aligned}$$

and the corresponding persistence conditions are

$$\begin{aligned} M(\phi_1)+M(\phi_1+\phi_2+\phi_3)+k\,M(\phi_1+\phi_2) &= 0 \\ M(\phi_2)+M(\phi_1+\phi_2+\phi_3)+k[M(\phi_1+\phi_2)+M(\phi_2+\phi_3)] &= 0 \\ M(\phi_3)+M(\phi_1+\phi_2+\phi_3)]+k\,M(\phi_2+\phi_3) &= 0 \end{aligned}$$

This case coincides with the 1D 4-site $r = 3$ chain case, with $k_3 = k_1 = 1$ and $k_2 = k$. Hence, the results

(both for the persistence and the stability of the solutions) are a special case of the previous section. All the existing multibreather families of this configuration are depicted in fig. 14.

In this diagram we can observe the appearance of $\{\phi_1 = \phi_2 = \phi_3 = \pi/2\}$ family, which is the vortex solution of the classical square Klein-Gordon lattice; see e.g., the relevant discussion in [21]. In addition, there are several phase-shift families, the stability of which will be analyzed below. Interestingly, all these phase-shift breathers cease to exist at a critical value of $k = k_{cr}^{(2)} = 1.03549$ except of the vortex one.

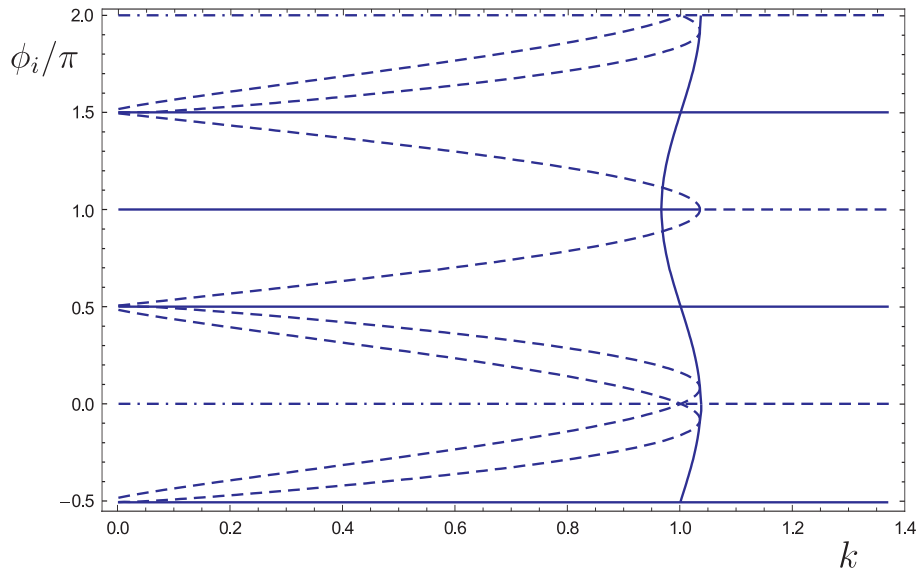

Figure 14: [Color online] In this diagram, the various multibreather families of the square lattice configuration, are depicted. The value of k determines the strength of the coupling in the diagonal direction. For a more detailed description of the particular families one can also refer to Fig. 15.

The mutibreather families that are supported by the present configuration are described in what follows.

- $\{\phi_1 = \phi_2 = \phi_3 = 0\}$ (in-phase) It is shown in Fig.15(a). It possesses 3 positive χ_z independently of the value of k_2.
- $\{\phi_1 = \phi_2 = \phi_3 = \pi/2\}$ (vortex). It is shown in Fig.15(a). It has no positive χ_z independently of the value of k_2 and does not interact (i.e., collide) with any other family of solutions.
- $\{\phi_1 = \phi_2 = \phi_3 = \pi\}$ (anti-phase). It is shown in Fig.15(a). It has no positive χ_z for $k < k_{cr}^{(1)} = 0.96572$, while for $k > k_{cr}^{(1)}$ it acquires 2 positive χ_z.
- $\{\phi_1 = \phi_3 = \pi,\ \phi_2 = \phi\}$ (phase-shift 1). It is represented by in Fig.15(b) $\phi_1 = \phi_3 = (1)$ and $\phi_2 = (2)$ or $\phi_1 = \phi_3 = (1)$ and $\phi_2 = (3)$. It exists for $k_{cr}^{(1)} < k_2 < k_{cr}^{(3)}$. It bifurcates from the anti-phase family at $k = k_{cr}^{(1)}$ and possesses 3 negative χ_z for $k_{cr}^{(1)} < k < k_{cr}^{(2)} = 1.0344$. At $k_2 = k_{cr}^{(2)}$ it collides with the phase-shift 2 family in a bubcritical pitchfork bifurcation. So, for $k_{cr}^{(2)} < k < k_{cr}^{(3)}$ it possesses 2 negative and a positive χ_z. At $k = k_{cr}^{(3)}$ it collides with the mixed family.
- $\{\phi_1 = \phi_3 = \pi,\ \phi_2 = 0\}$ (mixed). It is shown in Fig.15(c). It has 2 positive χ_z for $k < k_{cr}^{(3)} = 1.0355$ and 1 positive χ_z for $k_2 > k_{cr}^{(3)}$.
- (phase-shift 2a) It is represented in Fig.15(d) by $\phi_1 = \phi_3 = (4)$ and $\phi_2 =(8)$ which collides with the $\phi_1 = \phi_3 = (5)$ and $\phi_2 =(6)$ for $k_2 = k_{cr}^{(2)}$ and have 1 positive χ_z.

- (phase-shift 2b) It is represented in Fig.15(d) by $\phi_1 = \phi_3 = (4)$ and $\phi_2 =(9)$ which collides with the $\phi_1 = \phi_3 = (5)$ and $\phi_2 =(7)$ for $k_2 = k_{cr}^{(2)}$ and have 1 positive χ_z.

Notes on Figs. 14 and 15:

1. At $k = k_{cr}^{(2)}$ the $\phi_2 = (3)$ branch of the phase-shift 1 family collides with the phase-shift 2a family, while the the $\phi_2 = (2)$ branch of the phase-shift 1 family collides with the symmetric (and equivalent) of branches $\phi_2 = (7)$ and $\phi_2 = (9)$ of the phase-shift 2b family.
2. At $k = 0$ the phase-shift 2 family approaches very much the vortex family, so it is plausible to expect that at that point they coincide. Yet, there is a small difference in the values of ϕ_i of the two families due to the nonlinear character of the oscillators constituting the lattice, i.e., due to the existence of an infinity of terms in the development (4). For a smaller frequency of oscillation, the nonlinear character of the oscillation becomes stronger, hence the terms after the first in (4) become larger and the two families are more clearly separated.

8. Discussion - Comparison with the DNLS results

It should be noted here that a number of results similar to the ones presented herein have been recently presented in the context of the DNLS equation e.g. in [27, 28]. The setting of the DNLS essentially reflects a special case example of our Klein-Gordon calculation where instead of the existence and stability conditions reflecting a sum over *all* the harmonics due to the U(1) invariance of the underlying model, only the first harmonic is present. Nevertheless, the latter is sufficient to induce a number of the conclusions that we inferred herein. In particular, next-nearest neighbor interactions create phase-shift multibreathers (which were also parallelized to discrete vortex breathers in hexagonal lattices), as illustrated in [27]. As also shown in the same work, the long range interactions may drastically affect the stability properties of two-dimensional discrete vortices (in square lattices). On the other hand, the work of [28] provided a different analytical handle, via variational approximations, on the solutions that arise in settings with long range interactions. Furthermore, it was able to capture phenomena (both analytically and numerically) such as the supercritical or subcritical pitchfork bifurcations for such phase-shift multibreather solutions with NNN interactions. For instance, in the DNLS case the supecritical bifurcation leading to the emergence of such solutions would happen precisely at $k = 0.5$ (due to the relevance of just the first harmonic) and not at $k = 0.48286$ as obtained here in section IV B for the Klein-Gordon case. Nevertheless, the basic phenomenology remains intact.

It should also be noted here that the DNLS enables a wealth of additional results on the existence of localized modes e.g., based on homoclinic orbits and map type approaches [39], as well as on their asymptotic stability e.g., based on dispersive decay estimates [40]. Nevertheless, there are techniques that are common to both DNLS and Klein-Gordon type lattices, including the ones of continuation from the anti-continuum limit as used here. Another class of such common techniques, but from the "opposite limit", namely the continuum has been developed for the DNLS, with a recent example being the work of [41]. There, the use of ideas from finite element methods and variational analysis has enabled a proof of convergence to the ground state and a characterization of the localization length. Using, once again, the analogies between the DNLS and Klein-Gordon lattices, the work of [42] enabled the extension of results of existence of DNLS localized modes [43] in the small amplitude, near-continuum limit to the breathers of the Klein-Gordon type of chains.

9. Conclusions

Classical Klein-Gordon chain with nearest neighbor interactions support multibreather solutions only with phase differences between successive oscillators of $\phi_i = 0, \pi$. There, the stability scenaria are specific and well known. For a KG chain with $P = \varepsilon \frac{\partial \omega}{\partial J} < 0$ the anti-phase configuration is the only stable one, while for $P = \varepsilon \frac{\partial \omega}{\partial J} > 0$ the in-phase configuration is the only stable multibreather solution.

On the other hand, in chains with long range interactions the picture is *substantially* different. First of all, in such chains, multibreathers with $\phi_i \neq 0, \pi$ (phase-shift multibreathers) can be supported in addition to the standard $\phi_i = 0, \pi$ ones. The existence of phase-shift multibreathers as well as the specific ϕ_i's of such profiles depend on the various coupling parameters ε_i within the chain. There are critical values of $k_i = \varepsilon_i/\varepsilon_1$ past which a bifurcation occurs (typically a supercritical pitchfork) and phase shift breathers begin to exist. Past this bifurcation point, the stability properties of the existing multibreathers are significantly modified, although this also depends on the particular (soft or hard) nature of the nonlinearity. As, however, additional parameters are tuned (e.g., higher ranges of neighbor interactions), it is also possible for such phase-shift solutions to terminate in subcritical pitchfork bifurcations.

These results are not unique to the realm of one-dimensional lattices with higher range of interactions. They can also be developed for two-dimensional square lattices in which case they may lead to bifurcations or terminations of the families of discrete vortices which arise therein. Such vortices sustained by the two-dimensional analogs of the lattice can be of either a symmetric or asymmetric type. In particular, in the case considered herein, the presence of diagonal coupling within the square was critical in inducing the emergence of asymmetric such patterns.

This study opens a number of a directions for further investigation. Firstly, it would be very relevant to examine particular functional forms of the decay of the long range interactions (e.g., exponentially or polynomially decaying ones) to identify whether any systematic conclusions can be derived on the basis of such decay laws. As one such example, where the nature of the interactions plays a critical role on the properties of the localized modes, we mention the work of [44] on single-site localized modes of the DNLS with algebraically decaying interactions showing a crossover in their decay properties, and a modification of their existence energy thresholds as a function of the exponent of the algebraic decay of the interactions. Secondly, it would also be very interesting to examine the interplay of the geometry of higher dimensional lattices (and the interactions that they present) with the strength of the long range interactions that can be considered therein and to try to derive some general conclusions about the possible stable/unstable discrete soliton and discrete vortex solutions. Finally, an important and immediate direction that can be followed with the results of the paper in hand could be the effect of long-range interaction in phase-shift phonobreathers, whose stability for nearest-neighbor interaction was considered in [32]. A physical application of relevance and worthwhile of further investigation concerns the biological models for DNA [45, 46] or protein alpha-helices [47], where dipole long-range interactions are relevant.

Acknowledgments

The contribution of VK and VR in this research has been partially co-financed by the European Union (European Social Fund ESF) and Greek national funds through the Operational Program "Education and Lifelong Learning" of the National Strategic Reference Framework (NSRF) - Research Funding Program: THALES. Investing in knowledge society through the European Social Fund.

PGK gratefully acknowledges support from the National Science Foundation, under grants DMS-0806762, CMMI-1000337, and from the Alexander von Humboldt Foundation as well as from the Alexander S. Onassis Public Benefit Foundation.

JC acknowledges financial support from the MICINN project FIS2008-04848.

[1] A. J. Sievers, S. Takeno, Intrinsic localized modes in anharmonic crystals, Physical Review Letters 61 (1988) 970–973.
[2] J. B. Page, Asymptotic solutions for localized vibrational modes in strongly anharmonic periodic systems, Phys. Rev. B 41 (1990) 7835.
[3] R. S. MacKay, S. Aubry, Proof of the existence of breathers for time-reversible or Hamiltonian networks of weakly coupled oscillators, Nonlinearity 7 (1994) 1623.
[4] M. Peyrard, Nonlinear dynamics and statistical mechanics of DNA, Nonlinearity 17 (2004) R1.
[5] Y. S. Kivshar, G. P. Agrawal, Optical solitons: from fibers to photonic crystals, Academic Press, San Diego, 2003.
[6] G. Bartal, O. Cohen, T. Schwartz, O. Manela, F. B., M. Segev, H. Buljan, N. K. Efremidis, Spatial photonics in nonlinear waveguide arrays, Opt. Express 13 (2005) 1780.
[7] F. Lederer, G. I. Stegeman, D. Christodoulides, G. Assanto, M. Segev, Y. Silberberg, Discrete solitons in optics, Phys. Rep. 463 (2008) 1.
[8] M. Sato, B. E. Hubbard, A. J. Sievers, Nonlinear energy localization and its manipulation in micromechanical oscillator arrays, Rev. Mod. Phys. 78 (2006) 137.

[9] O. Morsch, M. O. Oberthaler, Dynamics of bose-einstein condensates in optical lattices, Rev. Mod. Phys. 78 (2006) 179.
[10] S. Sen, J. Hong, J. Bang, E. Avalos, E. Doney, Solitary waves in the granular chain, Phys. Rep. 462 (2008) 21.
[11] S. Flach, C. R. Willis, Discrete breathers, Phys. Rep. 295 (1998) 182.
[12] R. S. MacKay, Discrete breathers: classical and quantum, Physica A 288 (2000) 174–198.
[13] S. Flach, A. V. Gorbach, Discrete breathers - Advances in theory and applications, Phys. Rep. 467 (2008) 1.
[14] S. Aubry, Breathers in nonlinear lattices: existence, linear stability and quantization, Physica D 103 (1997) 201–250.
[15] J. F. R. Archilla, J. Cuevas, B. Sánchez-Rey, A. Álvarez, Demonstration of the stability or instability of multibreathers at low coupling, Physica D 180 (2003) 235.
[16] J. Cuevas, J. F. R. Archilla, F. R. Romero, Effect of the introduction of impurities on the stability properties of multibreathers, Nonlinearity 18 (2005) 76.
[17] T. Ahn, R. S. MacKay, J.-A. Sepulchre, Dynamics of relative phases: Generalised multibreathers, Nonlinear Dynamics 25 (2001) 157–182.
[18] R. S. MacKay, Slow manifolds, in: T. Dauxois, A. Litvak-Hinenzon, R. S. MacKay, A. Spanoudaki (Eds.), Energy Localisation and Transfer, World Scientific, 2004, pp. 149–192.
[19] R. S. MacKay, J.-A. Sepulchre, Effective Hamiltonian for travelling discrete breathers, Journal of Physics A 35 (2002) 3985–4002.
[20] V. Koukouloyannis, P. G. Kevrekidis, On the stability of multibreathers in Klein–Gordon chains, Nonlinearity 22 (2009) 2269.
[21] J. Cuevas, V. Koukouloyannis, P. G. Kevrekidis, J. F. R. Archilla, Multibreather and vortex breather stability in Klein–Gordon lattices: Equivalence between two different approaches, Int. J. Bifur. Chaos 21 (2011) 2161.
[22] D. E. Pelinovsky, A. Sakovich, Multi-site breathers in Klein-Gordon lattices: stability, resonances and bifurcations, arXiV:1111.2557 (2011).
[23] K. Yoshimura, Existence and stability of discrete breathers in diatomic fermi-pasta-ulam type lattices, Nonlinearity 24 (2011) 293.
[24] M. Feckan, V. M. Rothos, Travelling waves of discrete nonlinear Schrödinger equations with nonlocal interactions, Applicable Analysis 89 (2010) 1387–1411.
[25] V. Koukouloyannis, Non-existence of phase-shift multibreathers in one-dimensional klein-gordon lattices with nearest-neighbor interactions, (submitted for publication).
[26] P. G. Kevrekidis, The discrete nonlinear Schrödinger equation, Springer-Verlag, Berlin, 2009.
[27] P. G. Kevrekidis, Non-nearest-neighbor interactions in nonlinear dynamical lattices, Phys. Lett. A 373 (2009) 3688.
[28] C. Chong, R. Carretero-Gonzalez, B. A. Malomed, P. G. Kevrekidis, Variational approximations in discrete nonlinear Schrödinger equations with next-nearest-neighbor couplings, Physica D 240 (2011) 1205.
[29] J.-A. Sepulchre, R. S. MacKay, Localized oscillations in conservative or dissipative networks of weakly coupled autonomous oscillators, Nonlinearity 10 (3) (1997) 679–713.
[30] V. Koukouloyannis, S. Ichtiaroglou, Existence of multibreathers in chains of coupled one-dimensional hamiltonian oscillators, Physical Review E - Statistical, Nonlinear, and Soft Matter Physics 66 (6) (2002) 066602.
[31] V. Koukouloyannis, R. S. MacKay, Existence and stability of 3-site breathers in a triangular lattice, J. Phys. A: Math. Gen. 38 (2005) 1021.
[32] J. Cuevas, J. F. R. Archilla, F. R. Romero, Stability of non-time-reversible phonobreathers, J. Phys. A.: Math. Theor. 44 (2011) 035102.
[33] T. Ahn, Multisite oscillations in networks of weakly coupled autonomous oscillators, Nonlinearity 11 (1998) 965–989.
[34] D. Bambusi, Exponential stability of breathers in Hamiltonian networks of weakly coupled oscillators, Nonlinearity 9 (1996) 433–457.
[35] V. Koukouloyannis, T. T., G. Voyatzis, A method for studying the stability and the existence of discrete breathers in a chain of coupled symplectic maps, Nonlinear Phenomena in Complex Systems 11 (2) (2008) 233–240.
[36] D. Bambusi, Some stability properties of breathers in hamiltonian networks of oscillators, Physica D 119 (1998) 47–55.
[37] V. Koukouloyannis, P. G. Kevrekidis, K. J. H. Law, I. Kourakis, D. J. Frantzeskakis, Existence and stability of multisite breathers in honeycomb and hexagonal lattices, J. Phys. A: Math. Theor. 43 (2010) 235101.
[38] N. K. Efremidis, Discrete solitons in nonlinear zigzag optical waveguide arrays with tailored diffraction properties, Phys. Rev. E 65 (2002) 056607.
[39] W. . Qin, X. Xiao, Homoclinic orbits and localized solutions in nonlinear Schrödinger lattices, Nonlinearity 20 (10) (2007) 2305–2317.
[40] T. Mizumachi, D. Pelinovsky, On the asymptotic stability of localized modes in the discrete nonlinear Schrödinger equation, Discrete Contin. Dyn. Syst. Ser. S 5 (2012) 971–987.
[41] T. Penati, S. Paleari, Breathers and q-breathers: Two sides of the same coin, SIAM J. Applied Dynamical Systems 11 (1) (2012) 1–30.
[42] D. Bambusi, S. Paleari, T. Penati, Existence and continuous approximation of small amplitude breathers in 1d and 2d klein-gordon lattices, Applicable Analysis 89 (9) (2010) 1313–1334.
[43] D. Bambusi, T. Penati, Continuous approximation of breathers in one- and two-dimensional dnls lattices, Nonlinearity 23 (1) (2010) 143–157.
[44] S. Flach, Breathers on lattices with long range interaction, Phys. Rev. E 58 (4) (1998) R4116–R4119.
[45] J. Cuevas, J. F. R. Archilla, Y. B. Gaididei, F. R. Romero, Moving breathers in a DNA model with competing short- and long-range dispersive interactions, Physica D 163 (2002) 106–126.
[46] J. Cuevas, E. B. Starikov, J. F. R. Archilla, D. Hennig, Moving breathers in bent DNA with realistic parameters, Mod. Phys. Lett. B 18 (2004) 1319–1326.

[47] J. F. R. Archilla, Y. B. Gaididei, P. L. Christiansen, J. Cuevas, Stationary and moving breathers in a simplified model of curved alphahelix proteins, J. Phys. A.: Math. Gen. 35 (2002) 8885.

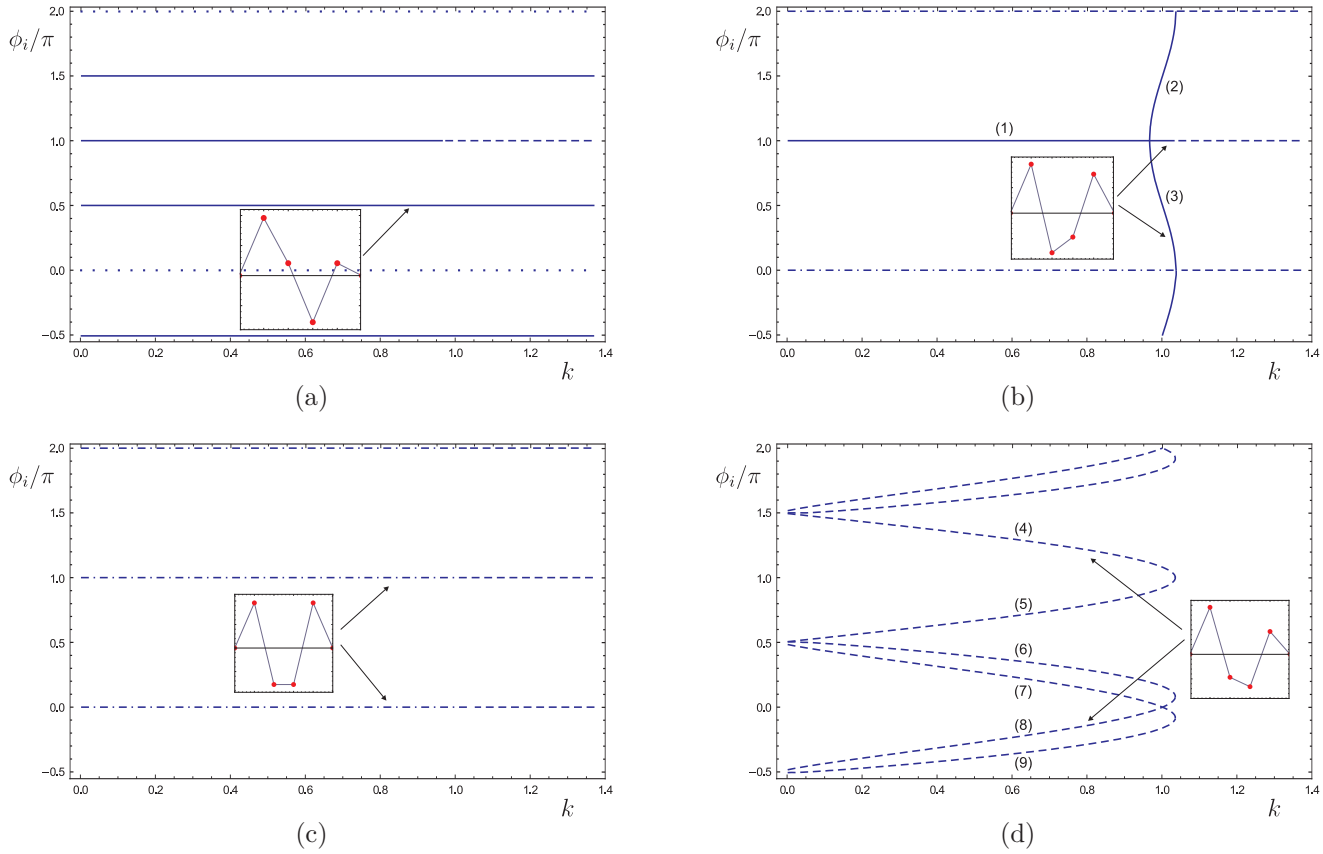

Figure 15: [Color online] The various multibreather families that consist Fig. 14 are depicted. Portraits of the configuration of the central oscillators for the different multibreather families are shown as insets in the corresponding diagrams. Note that, for better presentation, instead of showing the the 4 central oscillators in a square configuration, we show their 1D equivalent. The line (or curve) type in the figures depends on the number of positive χ_z the corresponding family possesses: no positive χ_z corresponds to solid line, 1 positive χ_z corresponds to dashed line, 2 to dashed-dotted and 3 to dotted line. In **(a)** three families are shown. The first family is the in-phase one $\{\phi_1 = \phi_2 = \phi_3 = 0 \text{ or } 2\pi\}$, which possesses 3 positive χ_z. The second family is the vortex $\{\phi_1 = \phi_2 = \phi_3 = \pi/2 \text{ (or } 3\pi/2)\}$ family. It possesses no positive χ_z. The third family is the anti-phase one $\{\phi_1 = \phi_2 = \phi_3 = \pi\}$. This family possesses no positive χ_z for $k < k_{cr}^{(1)} = 0.96572$, while for $k > k_{cr}^{(1)}$ it acquires 2 positive χ_z. At this point it bifurcates to provide the phase-shift 1 family. In this figure only the inset of the vortex family is present because all the others are the same as the ones presented for the equivalent 1D configuration, in figs. 10. In **(b)** the phase-shift 1 $\{\phi_1 = \phi_3 = \pi,\ \phi_2 = \phi\}$ family is shown, which exists for $k_{cr}^{(1)} < k < k_{cr}^{(3)} = 1.03549$. It is depicted by $\phi_1 = \phi_3 =$ (1) and $\phi_2 =$ (2) or $\phi_1 = \phi_3 =$ (1) and $\phi_2 =$ (3). It possesses no positive χ_z for $k_{cr}^{(1)} < k < k_{cr}^{(2)} = 1.0344$. At $k = k_{cr}^{(2)}$ it collides with the phase-shift 2 family. For $k_{cr}^{(2)} < k < k_{cr}^{(3)}$ the family possesses 1 positive χ_z. At $k = k_{cr}^{(3)}$ it collides with the mixed family. In **(c)** the mixed family $\{\phi_1 = \phi_3 = \pi,\ \phi_2 = 0\}$ is depicted. It has 2 positive χ_z for $k < k_{cr}^{(2)}$ and 1 positive χ_z for $k_2 > k_{cr}^{(3)}$. Finally in **(d)** two phase-shift families are depicted. The phase phase-shift 2a family, which is represented by $\phi_1 = \phi_3 =$ (4) and $\phi_2 =$(8) which collides with the $\phi_1 = \phi_3 =$ (5) and $\phi_2 =$(6) for $k_2 = k_{cr}^{(2)}$, and the phase-shift 2b family which is represented by $\phi_1 = \phi_3 =$ (4) and $\phi_2 =$(9) which collides with the $\phi_1 = \phi_3 =$ (5) and $\phi_2 =$(7) for $k_2 = k_{cr}^{(2)}$. They both possess 1 positive χ_z.